



ARTICLE

Glutamylation of deubiquitinase BAP1 controls self-renewal of hematopoietic stem cells and hematopoiesis

Zhen Xiong^{1,2*}, Pengyan Xia^{1*}, Xiaoxiao Zhu^{3*}, Jingjing Geng^{1,2}, Shuo Wang¹, Buqing Ye¹, Xiwen Qin^{1,2}, Yuan Qu^{1,2}, Luyun He^{1,2}, Dongdong Fan³, Ying Du¹, Yong Tian^{2,3} , and Zusen Fan^{1,2} 

All hematopoietic lineages are derived from a limited pool of hematopoietic stem cells (HSCs). Although the mechanisms underlying HSC self-renewal have been extensively studied, little is known about the role of protein glutamylation and deglutamylation in hematopoiesis. Here, we show that carboxypeptidase CCP3 is most highly expressed in BM cells among CCP members. CCP3 deficiency impairs HSC self-renewal and hematopoiesis. Deubiquitinase BAP1 is a substrate for CCP3 in HSCs. BAP1 is glutamylated at Glu651 by TTLL5 and TTLL7, and BAP1-E651A mutation abrogates BAP1 glutamylation. BAP1 glutamylation accelerates its ubiquitination to trigger its degradation. CCP3 can remove glutamylation of BAP1 to promote its stability, which enhances *Hoxa1* expression, leading to HSC self-renewal. *Bap1*^{E651A} mice produce higher numbers of LT-HSCs and peripheral blood cells. Moreover, TTLL5 and TTLL7 deficiencies sustain BAP1 stability to promote HSC self-renewal and hematopoiesis. Therefore, glutamylation and deglutamylation of BAP1 modulate HSC self-renewal and hematopoiesis.

Introduction

Many blood components, including erythrocytes, neutrophils, and megakaryocytes, are short-lived and are constantly regenerated. All hematopoietic lineages are derived from a limited pool of hematopoietic stem cells (HSCs), which represents one of the most canonical adult stem cells (Orkin and Zon, 2008). At the very top of hematopoietic hierarchy is the long-term HSC (LT-HSC). LT-HSCs possess pluripotency to generate all blood cells throughout their lifetime, and they keep predominantly quiescent at G₀ phase (Wilson et al., 2008). Oxidative stress (Tothova et al., 2007), infection (Sato et al., 2009), and aging (Flach et al., 2014; Takubo et al., 2010) can activate HSCs to enter the cell cycle and replenish blood cells, but excessive mobilization burdens HSCs and renders them exhausted. LT-HSCs give rise to daughter stem cells through self-renewal, as well as downstream short-term HSCs and multipotent progenitors (MPPs), along with progressively bereaving self-renewal ability (Rossi et al., 2012). Thus, HSCs are essential to guarantee lifelong hematopoiesis.

Protein posttranslational modifications, such as methylation, phosphorylation, ubiquitination, and sumoylation, have been reported to participate in regulating hematopoiesis (Cimmino

et al., 2017; Liu et al., 2014; Nakagawa et al., 2015; Zhu et al., 2011). Glutamylation is another posttranslational modification that was initially identified on tubulins (Eddé et al., 1990). By adding glutamate side chains onto the γ -carboxyl groups of glutamic acid residues of the target proteins, glutamylation alters charge characteristics, protein-protein interaction, stability, and activity of the modified targets. As a reversible process of glutamylation, a group of tubulin tyrosine ligase-like (TTLL) enzymes add the glutamate side chains (Janke et al., 2005), while members of the cytosolic carboxypeptidase (CCP) family of enzymes remove them (Rogowski et al., 2010). Given that TTLLs and CCPs are reversible-modification enzyme members with unique distributions, they might harbor nonredundant roles in the regulation of cellular processes by orchestrating glutamylation and deglutamylation of target proteins (Janke, 2014). Besides glutamylation of tubulin, several other target proteins have been recently identified to be glutamylated (van Dijk et al., 2008). We previously reported that Mad2 can be glutamylated to modulate megakaryocyte maturation (Ye et al., 2014). IL-7R α is glutamylated to regulate the development of group 3 innate lymphoid cells (ILC3s; Liu et al., 2017a). Cyclic GMP-AMP

¹Key Laboratory of Infection and Immunity of Chinese Academy of Sciences, Chinese Academy of Sciences Center for Excellence in Biomacromolecules, Institute of Biophysics, Chinese Academy of Sciences, Beijing, China; ²University of Chinese Academy of Sciences, Beijing, China; ³Key Laboratory of RNA Biology of Chinese Academy of Sciences, Institute of Biophysics, Chinese Academy of Sciences, Beijing, China.

*Z. Xiong, P. Xia, and X. Zhu contributed equally to this paper; Correspondence to Zusen Fan: fanz@moon.ibp.ac.cn; Yong Tian: ytian@ibp.ac.cn.

© 2019 Xiong et al. This article is distributed under the terms of an Attribution-Noncommercial-Share Alike-No Mirror Sites license for the first six months after the publication date (see <http://www.rupress.org/terms/>). After six months it is available under a Creative Commons License (Attribution-Noncommercial-Share Alike 4.0 International license, as described at <https://creativecommons.org/licenses/by-nc-sa/4.0/>).

synthase (cGAS) can be glutamylated to inhibit its synthase activity during DNA virus infections (Xia et al., 2016). However, how glutamylation regulates HSC self-renewal is still unclear.

BAP1 is a deubiquitinase that is involved in many cellular processes, including transcription regulation, cell cycle, proliferation, DNA damage, and cell death (Bononi et al., 2017). BAP1 mutations have been reported to be implicated in oncogenesis of several malignancies (Pilarski et al., 2014). Moreover, cancer-derived BAP1 mutations that abolish autodeubiquitination and promote its cytoplasmic sequestration abolish its function as a tumor suppressor (Mashtalir et al., 2014). Cytoplasmic BAP1 can deubiquitylate and stabilize IP3R3, which modulates calcium release from endoplasmic reticulum and enhances apoptosis (Bononi et al., 2017). Deletion of BAP1 in the hematopoietic system causes myelodysplastic syndrome (Dey et al., 2012). Here, we show that CCP3 deficiency impairs HSC self-renewal and hematopoiesis. CCP3 can deglutamylate BAP1 to promote its stability, which enhances *Hoxa1* expression, leading to HSC self-renewal. BAP1 glutamylation at Glu651 is catalyzed by TLL5 and TLL7. Moreover, TLL5 and TLL7 deficiencies sustain BAP1 stability to promote HSC self-renewal and hematopoiesis.

Results

CCP3 deficiency impairs hematopoiesis and HSC self-renewal

We previously demonstrated that CCP6 deficiency in mice causes underdeveloped megakaryocytes and dysfunctional platelets (Ye et al., 2014). To further explore how glutamylation regulated hematopoiesis, we tested expression levels of *Ccps* in mouse bone marrow (BM). We found that only *Ccp3* was most highly expressed in BM cells (Fig. 1 A). Of note, *Ccp3*-deleted (*Ccp3*^{-/-}) mice displayed splenomegaly and increased spleen weight (Fig. 1 B). Moreover, *Ccp3*^{-/-} mice showed disordered structure of splenic white pulp, suggesting extramedullary hematopoiesis (Fig. S1 A). In addition, *Ccp3*^{-/-} mice decreased cell counts of erythrocytes, myeloid cells, and lymphocytes in peripheral blood (Fig. 1 C, Fig. S1 B, and Table S1). By contrast, CCP4-deficient mice displayed normal spleen and cell numbers of blood lineages we tested (Fig. 1 B and Fig. S1, A and B). Consequently, *Ccp3*^{-/-} mice showed reduced BM cellularity compared with *Ccp3*^{+/+} mice (Fig. 1 D and Fig. S1 C).

Blood cells can be replenished a short time after being damaged. To determine this regeneration capacity in *Ccp3*^{-/-} mice, we used 5-fluorouracil (5-FU) to eliminate proliferating cells and enforce hematopoietic regeneration. We observed that peripheral white blood cell (WBC) numbers in *Ccp3*^{-/-} mice were dramatically reduced after 5-FU treatment, and they failed to replenish blood cells and BM cells (Fig. S1, D and E). Furthermore, *Ccp3*^{-/-} mice could not survive three rounds of continuous 5-FU treatment, while WT mice could (Fig. S1 F). We used carboxypeptidase inhibitor phenanthroline (Rogowski et al., 2010) to suppress CCP3 activity in WT mice during 5-FU treatment. We noticed that phenanthroline treatment showed phenotypes similar to *Ccp3*^{-/-} mice (Fig. S1, G and H), suggesting CCP3 enzymatic activity is indispensable for hematopoietic regeneration capacity.

HSCs dominate the ultimate source of blood cell regeneration. We found that *Ccp3* was most highly expressed in HSCs

compared with other lineages (Fig. S1 I). Of note, *Ccp3*^{-/-} mice showed decreased total numbers and total frequencies of LSKs (Lin⁻Sca-1⁺c-Kit⁺), MPPs (Lin⁻Sca-1⁺c-Kit⁺CD48⁺CD150⁻), and LT-HSCs (Lin⁻Sca-1⁺c-Kit⁺CD48⁺CD150⁺; Fig. 1 E and Fig. S1 J). HSCs give rise to common myeloid progenitors (CMPs) and common lymphoid progenitors (CLPs) and further differentiate into mature blood components hierarchically (Xia et al., 2015). Consequently, *Ccp3*^{-/-} mice showed decreased numbers of CMPs and CLPs as well as blood cell counts (Fig. 1 F, Fig. S1 K, and Table S1). In addition, we performed a CFU assay to test the role of CCP3 in the activity of hematopoietic stem and progenitor cells (HSPCs) in vitro. We observed that *Ccp3*^{-/-} BM cells produced fewer colonies compared with those of *Ccp3*^{+/+} littermate control mice (Fig. 1 G). Moreover, *Ccp3*^{-/-} BM cells generated much lower numbers of colonies in secondary replating formation (Fig. 1 H). To determine in vitro differentiation and maintenance ability of *Ccp3*-deficient LT-HSCs, we performed serial plating CFU assays using *Ccp3*^{+/+} and *Ccp3*^{-/-} LT-HSCs. CFU formations of primary plating were comparable between *Ccp3*^{+/+} and *Ccp3*^{-/-} LT-HSCs (Fig. 1 I). However, *Ccp3*^{-/-} LT-HSCs produced much fewer CFUs in successive plating (Fig. 1 I), suggesting *Ccp3*^{-/-} LT-HSCs disrupt maintenance and self-renewal ability. A single LT-HSC can undergo population expansion for a certain time after being cultured with cytokine cocktail (Himburg et al., 2010). We found that *Ccp3*^{-/-} LT-HSCs lost their expanding and regenerating ability through single-cell culture assay (Fig. 1 J). In addition, phenanthroline treatment impeded WT LT-HSC expansion, and the CCP enzyme agonist CoCl₂ (Berezniuk et al., 2012) remarkably increased their expansion. However, with phenanthroline or CoCl₂ treatment, expansion abilities of *Ccp3*^{-/-} LT-HSCs were unchanged, suggesting a specific role of CCP3 in the regulation of LT-HSC expansion (Fig. 1 J). Of note, *Ccp3*^{-/-} LT-HSCs failed to be recovered after 5-FU treatment (Fig. S1 L). Finally, we observed that *Ccp3*^{-/-} mice had fewer quiescent LT-HSCs and greater number of cycling HSCs (Fig. 1 K). Of note, *Ccp3*^{-/-} LT-HSCs did not show apparent cell death (Fig. 1 L). Collectively, CCP3 deficiency impairs hematopoiesis and HSC self-renewal.

CCP3 intrinsically regulates HSC self-renewal

We next sought to determine whether CCP3 deficiency-mediated impairment of hematopoiesis was intrinsic or extrinsic. We transplanted CD45.2⁺ *Ccp3*^{+/+} or *Ccp3*^{-/-} BM cells into lethally irradiated CD45.1⁺ recipients (Fig. 2 A). Engraftment of *Ccp3*^{-/-} BM cells decreased numbers of peripheral blood cells and BM cells (Fig. 2, B and C). Then we performed LT-HSC transplantation. We found that homing efficiency of *Ccp3*^{-/-} LT-HSCs was comparable to *Ccp3*^{+/+} LT-HSCs (Fig. S2 A). However, *Ccp3*^{-/-} LT-HSC transplantation generated fewer peripheral blood cells and BM cells and failed to maintain LT-HSC self-renewal and hematopoiesis, whereas transplantation of *Ccp3*^{+/+} LT-HSCs could produce normal numbers of peripheral blood cells and BM cells and maintain normal long-term hematopoiesis as well (Fig. 2, D and E; and Fig. S2, B and C).

We also performed competitive BM transplantation assays. We transplanted a 1:1 mixture of CD45.1⁺ WT and CD45.2⁺ *Ccp3*^{-/-} or *Ccp3*^{+/+} BM cells into lethally irradiated recipient mice (Fig. 2 F). Engraftment of *Ccp3*^{+/+} BM cells kept long-term

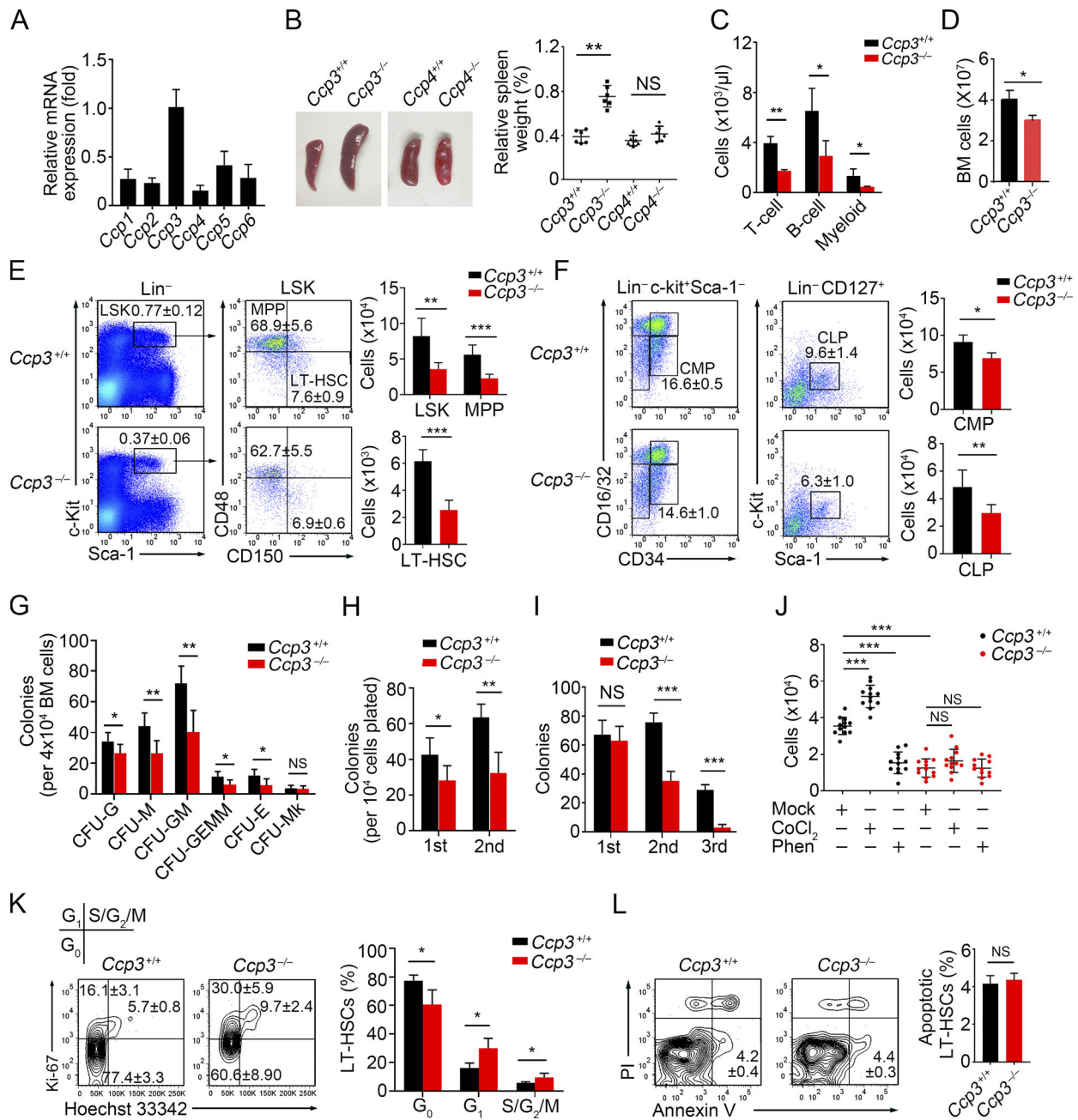


Figure 1. **Ccp3** deficiency impairs hematopoiesis and HSC pool. **(A)** mRNAs of BM cells from *Ccp* family (*Agtpbp1*, called *Ccp1* here; *Agbl2*, called *Ccp2* here; *Agbl3*, called *Ccp3* here; *Agbl1*, called *Ccp4* here; *Agbl5*, called *Ccp5* here; and *Agbl4*, called *Ccp6* here) were analyzed by quantitative real-time PCR (qPCR). Results were normalized to expression of endogenous *Actb* gene ($n = 5$). **(B)** Photographs of spleens from *Ccp3*^{+/+}, *Ccp3*^{-/-}, *Ccp4*^{+/+}, and *Ccp4*^{-/-} mice (left) and relative spleen weight (spleen/body) of respective mice (right). $n = 6$. **(C)** Peripheral blood cells from *Ccp3*^{+/+} and *Ccp3*^{-/-} mice were counted by flow cytometry. Numbers of T cells (CD3⁺), B cells (CD19⁺), and myeloid cells (CD11b⁺Gr-1⁺) were calculated ($n = 3$). **(D)** BM cell numbers in a femur of *Ccp3*^{+/+} and *Ccp3*^{-/-} mice were counted ($n = 6$). **(E)** Left: LSKs (Lin⁻Sca-1⁺c-Kit⁺), MPPs (Lin⁻Sca-1⁺c-Kit⁺CD48⁺CD150⁻), and LT-HSCs (Lin⁻Sca-1⁺c-Kit⁺CD48⁺CD150⁺) from *Ccp3*^{+/+} and *Ccp3*^{-/-} mice were analyzed by flow cytometry. Right: Total numbers of indicated cells in a femur were calculated ($n = 6$). **(F)** Left: CMP cells (Lin⁻Sca-1⁺c-Kit⁺CD34⁺CD16/32⁺) and CLP cells (Lin⁻CD127⁺Sca-1^{low}c-Kit^{low}) from *Ccp3*^{+/+} and *Ccp3*^{-/-} mice were assayed by flow cytometry. Right: Total numbers of the indicated cells in a femur were calculated ($n = 6$). **(G)** CFUs of granulocyte colonies (G), macrophage colonies (M), granulocyte-macrophage colonies (GM), granulocyte, erythroid, macrophage, and megakaryocyte colonies (GEMM), erythroid colonies (E), and megakaryocyte colonies (Mk) were scored 10 d after plating of *Ccp3*^{+/+} and *Ccp3*^{-/-} BM cells ($n = 6$). **(H)** 1×10^4 BM cells from *Ccp3*^{+/+} and *Ccp3*^{-/-} mice were plated for 7-d cultures, and 1×10^4 cells were replated for the next round of cultures. Colonies were counted every 7 d ($n = 6$). **(I)** 1×10^2 *Ccp3*^{+/+} and *Ccp3*^{-/-} LT-HSCs were sorted and plated for 7-d cultures, and then 2,000 cells were replated for a second and third round of plating. Colonies were counted every 7 d ($n = 6$). **(J)** *Ccp3*^{+/+} and *Ccp3*^{-/-} LT-HSCs were sorted for single-cell culture and counted after 7 d. CCP3 agonist CoCl₂ (10 μM) or inhibitor phenanthroline (1 μM) was added, respectively ($n = 12$). **(K)** Flow cytometry analysis of cell cycle of *Ccp3*^{+/+} and *Ccp3*^{-/-} LT-HSCs. Percentages of different cell cycle phases were calculated ($n = 4$). **(L)** Left: BM cells from *Ccp3*^{+/+} and *Ccp3*^{-/-} mice were stained with PI and Annexin V to analyze cell apoptosis. Right: Percentages of apoptotic cells (PI⁺, Annexin V⁺) were calculated ($n = 4$). Results are shown as means ± SD. *, $P < 0.05$; **, $P < 0.01$; ***, $P < 0.001$. Two-tailed Student's *t* test. Data in A–C and G–L are representative of three independent experiments. Data in D–F are pooled from three independent experiments.

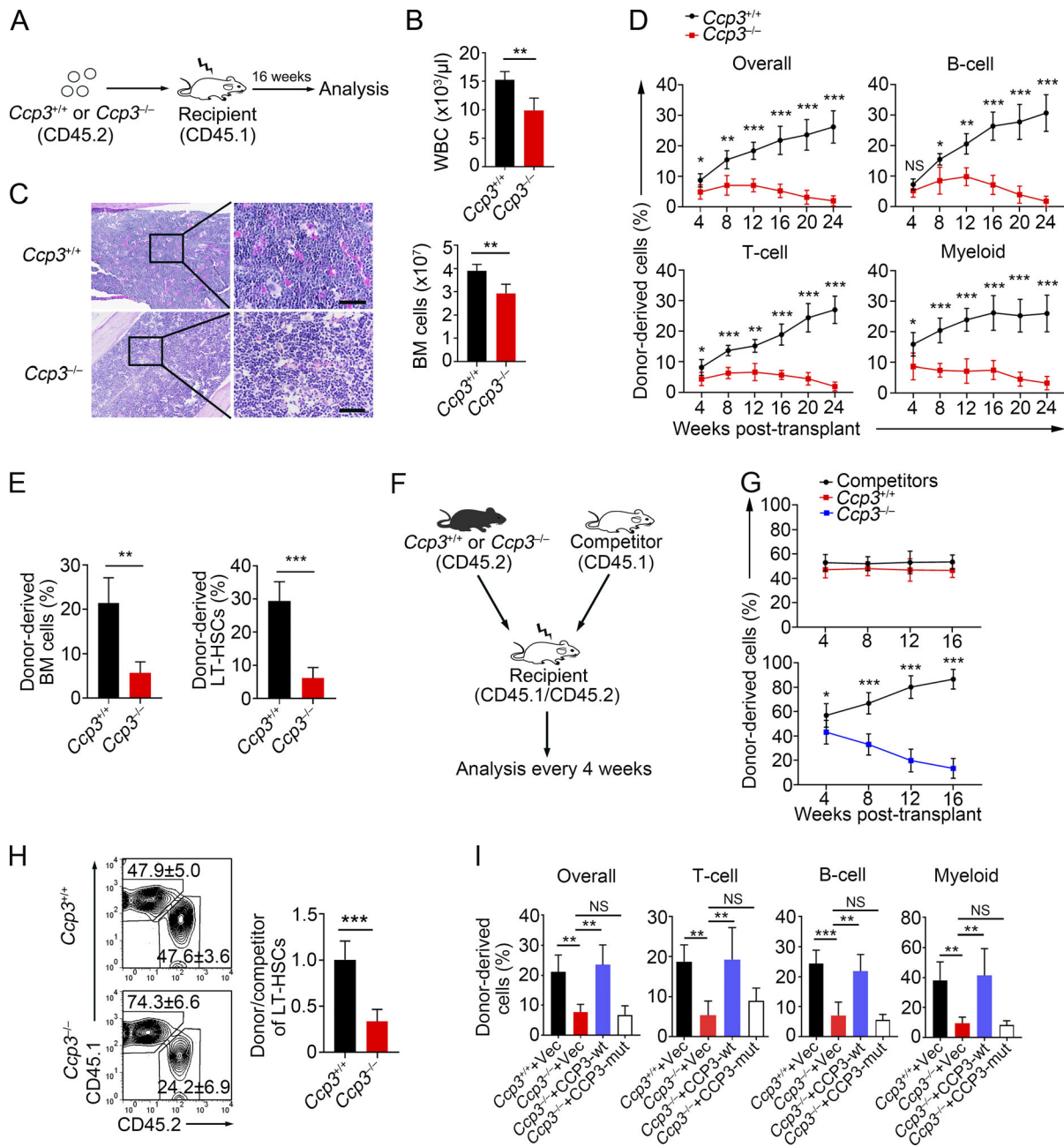


Figure 2. CCP3 is an intrinsic factor to regulate HSC self-renewal. (A) Schematic diagram of BM transplantation. 1×10^6 BM cells from *Ccp3*^{+/+} and *Ccp3*^{-/-} mice (CD45.2) were transplanted into lethally irradiated CD45.1 mice, followed by analysis 16 wk after BM transplantation. (B) Peripheral WBCs derived from transplanted *Ccp3*^{+/+} and *Ccp3*^{-/-} BM cells were counted 16 wk after BM transplantation ($n = 6$). (C) Left: H&E staining of BM sections from femurs of *Ccp3*^{+/+} and *Ccp3*^{-/-} BM transplanted recipient mice. Scale bars, 50 μ m. Right: BM cells were counted 16 wk after BM transplantation ($n = 6$). (D) 1×10^2 LT-HSCs from *Ccp3*^{+/+} and *Ccp3*^{-/-} mice were sorted and mixed with 5×10^5 BM helpers (CD45.1⁺CD45.2⁺), and then transplanted into lethally irradiated CD45.1 mice. Peripheral WBCs were analyzed by flow cytometry every 4 wk ($n = 5$). (E) Donor-derived BM cells (left) and LT-HSCs (right) were analyzed by flow cytometry 16 wk after LT-HSC transplantation ($n = 5$). (F) Schematic diagram of competitive BM transplantation. 1×10^6 *Ccp3*^{+/+} or *Ccp3*^{-/-} BM cells (CD45.2) were mixed with 1×10^6 competitors (CD45.1) and cotransplanted into lethally irradiated mice (CD45.1⁺CD45.2⁺). Peripheral WBCs were analyzed by flow cytometry every 4 wk. Donor-derived LT-HSCs were analyzed by flow cytometry 16 wk after transplantation. (G) Percentages of peripheral WBCs derived from *Ccp3*^{+/+} or *Ccp3*^{-/-} BM (CD45.2) cells and competitors (CD45.1) were analyzed by flow cytometry every 4 wk ($n = 6$). (H) Left: Flow cytometry analysis of LT-HSCs 16 wk after competitive BM transplantation. Right: Ratios of *Ccp3*^{+/+} or *Ccp3*^{-/-} LT-HSCs to competitors were calculated ($n = 6$). (I) CCP3-wt or enzymatic inactive CCP3 (CCP3-mut) were overexpressed in *Ccp3*^{-/-} LT-HSCs (CD45.2) with pMYs retrovirus. 1×10^2 GFP⁺ cells were sorted and mixed with 5×10^5 BM helpers for BM transplantation. Peripheral WBCs were analyzed by flow cytometry 16 wk after transplantation ($n = 5$). Results are shown as means \pm SD. *, $P < 0.05$; **, $P < 0.01$; ***, $P < 0.001$. Two-tailed Student's *t* test. Data are representative of three independent experiments.

balance with their competitors, whereas transplantation of *Ccp3*^{-/-} BM cells was gradually reduced during competition (Fig. 2 G). 16 wk after transplantation, transplanted *Ccp3*^{-/-} BM cells had reduced counts of peripheral blood cells and LT-HSCs compared with their WT competitors (Fig. 2, G and H). These results indicate that CCP3 is an intrinsic factor in regulating HSC self-renewal and hematopoiesis.

It has been reported that Glu540-to-Ala mutation abolishes deglutamylase activity of CCP3 (Tort et al., 2014). To examine whether CCP3 deficiency-mediated impairment of hematopoiesis was dependent on CCP3 enzymatic activity, we generated the Glu540-to-Ala mutation construct (CCP3-mut) and overexpressed it into *Ccp3*^{-/-} LT-HSCs, followed by reconstitution assay (Fig. S2 D). Through BM transplantation assay, we found that engraftment of LT-HSCs with CCP3-wt overexpression could restore hematopoiesis, whereas transplantation of LT-HSCs with CCP3-mut overexpression still abrogated hematopoiesis (Fig. 2 I). These data suggest that enzymatic activity of CCP3 is required for the regulation of hematopoiesis.

BAP1 is a substrate for CCP3

To further determine the molecular mechanism of CCP3-mediated hematopoiesis, we analyzed lysates of *Ccp3*^{-/-} or *Ccp3*^{+/+} LSK cells by immunoblotting with a glutamylation-specific antibody: GT335. The antibody GT335 specifically recognizes the branch points of glutamate side chains and detects all glutamylation forms of target proteins (Ye et al., 2018). After Western blot analysis, one band around 95 kD appeared in the lane of CCP3-deficient LSK lysates (Fig. 3 A). This band was undetectable in the corresponding lane location from the littermate control LSK lysates. Therefore, this band could be a potential candidate substrate for CCP3. To identify the candidate substrates of CCP3, we generated CCP3-mut through Glu540-to-Ala mutation. CCP3-wt and CCP3-mut were immobilized in Affi-Gel 10 resin to go through mouse BM lysates for affinity chromatography. The eluted fractions were resolved by SDS-PAGE, followed by silver staining. This band was present in the gel analyzing CCP3-mut and was cut for mass spectrometry, where the band was identified as BAP1 (Fig. 3 B and Fig. S3 A). BAP1 is a nuclear-localized deubiquitinating enzyme that participates in the regulation of development, cell proliferation, and tumor transformation (Bononi et al., 2017; Dey et al., 2012; Yu et al., 2010). However, how glutamylation of BAP1 regulates hematopoiesis is still unknown.

We next overexpressed Myc-tagged BAP1 and Flag-tagged CCP3-wt or CCP3-mut in HEK293T cells for coimmunoprecipitation assay. We observed that the Flag-tagged CCP3-mut could pull down the Myc-tagged BAP1. Furthermore, CCP3-mut was able to immunoprecipitate endogenous BAP1, whereas CCP3-wt could not (Fig. 3 D). Since CCP3-wt could remove glutamylation of BAP1, deglutamylated BAP1 could not bind to active CCP3-wt. In addition, endogenous BAP1 was highly glutamylated in *Ccp3*^{-/-} LSK lysates, while it was less glutamylated in *Ccp3*^{+/+} LSK lysates (Fig. 3 E). Finally, phenanthroline treatment remarkably increased BAP1 glutamylation, whereas CoCl₂ treatment almost abolished the glutamylation of BAP1 (Fig. 3 F). Collectively, BAP1 is indeed glutamylated in LSK cells.

BAP1 is glutamylated at Glu651 by TLL5 and TLL7

Nine glutamylase members of the TLL family have been recently identified (Garnham et al., 2015). We wanted to explore which TLL members catalyzed BAP1 in HSCs. We tested expression levels of these nine TLL members in HSCs and mature lineage cells. We observed that *Tll5* and *Tll7* were most highly expressed in LSKs, especially in LT-HSCs (Fig. 4 A). We then expressed mouse TLL5 and TLL7 in HEK293T cells and incubated them with recombinant mouse BAP1 for in vitro glutamylation assay. We noticed that BAP1 was highly glutamylated by TLL5 and TLL7 (Fig. 4, B and C). By contrast, CCP3 could remove the glutamylation of BAP1 (Fig. 4, B and C). These results indicate that BAP1 is glutamylated by TLL5 and TLL7, whose glutamylation is removed by CCP3.

Glutamylation has been found to be modified on the glutamate-rich stretches and acidic environment at the acceptor sites (van Dijk et al., 2008). We analyzed conservative amino acid sequences of BAP1 and screened out conserved identical glutamic acid residues for mutations (Fig. S3 B). Through in vitro glutamylation assay, we identified that only the Glu651-to-Ala mutation of BAP1 (BAP1-E651A) abolished its glutamylation, indicating that BAP1 is catalyzed by TLL5 and TLL7 at Glu651 (Fig. 4 D and Fig. S3, C and D). We next generated *Tll5*- and *Tll7*-deficient mice, as well as *Bap1*^{E651A} knock-in mutant mice via CRISPR-Cas9 technology (Fig. S3, E–G). As expected, we found that glutamylation of BAP1 was dramatically reduced in TLL5- and TLL7-deficient LSKs, and BAP1 failed to undergo glutamylation in *Bap1*^{E651A} knock-in mutant mice (Fig. 4 E). These data confirm that BAP1 is glutamylated by TLL5 and TLL7 at Glu651.

Of note, we observed that *Bap1*^{E651A} mice displayed an increased percentage and number of LT-HSCs and consequently increased numbers of peripheral blood cells and BM cells (Fig. 4, F and G). As expected, more LT-HSCs were kept in G₀ phase in *Bap1*^{E651A} mice (Fig. 4 H). Through serial LT-HSC transplantation, we noticed that engraftment of *Bap1*^{E651A} LT-HSCs could produce more LT-HSCs and peripheral blood cells (Fig. 4, I and J). We conclude that glutamylation negatively regulates BAP1 function in the regulation of HSC maintenance and hematopoietic reconstruction ability.

BAP1 glutamylation enhances its ubiquitination for degradation

It has been reported that the ubiquitin-conjugating enzyme UBE2O interacts with BAP1 to catalyze its ubiquitination (Mashtalir et al., 2014). We found that BAP1 protein level in *Ccp3*^{-/-} LSKs was markedly lower than that in *Ccp3*^{+/+} cells (Fig. 5 A). However, *Bap1* mRNA levels were comparable in *Ccp3*^{-/-} and *Ccp3*^{+/+} LSKs (Fig. 5 B). These data suggest that BAP1 glutamylation might facilitate its degradation. With cycloheximide (CHX) treatment, BAP1 in *Ccp3*^{-/-} LSKs was rapidly degraded, whereas BAP1 in *Ccp3*^{+/+} LSKs was more stable (Fig. 5 C). Of note, the proteasome inhibitor MG132 could impede BAP1 degradation (Fig. 5 C). These data suggest that BAP1 glutamylation facilitates its degradation. In addition, the interaction between BAP1 and UBE2O was confirmed by coimmunoprecipitation assay (Fig. 5 D). Moreover, BAP1 glutamylation enhanced their

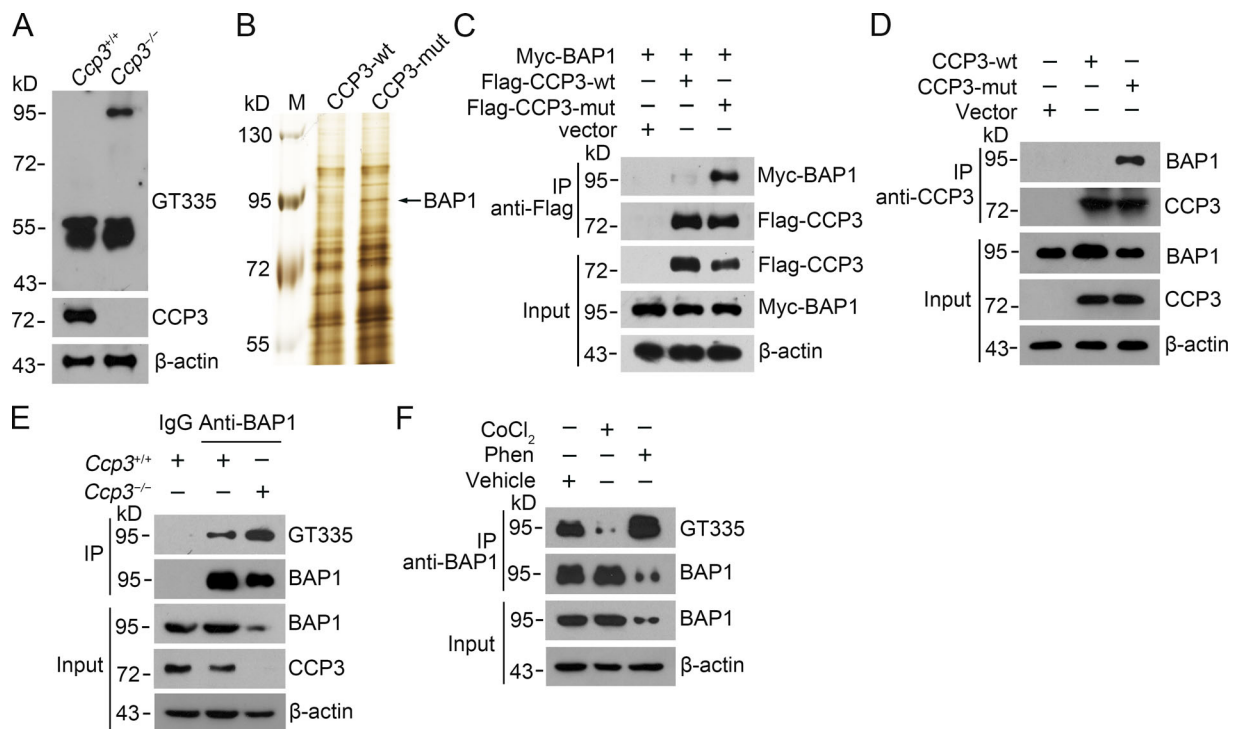


Figure 3. BAP1 is a substrate for CCP3 in HSCs. (A) 1×10^6 LSK cells from *Ccp3*^{+/+} and *Ccp3*^{-/-} BM were sorted via flow cytometry, followed by SDS-PAGE and Western blotting. Protein glutamylation was probed with GT335 antibody. (B) Recombinant CCP3-wt and enzymatic inactive CCP3 (CCP3-mut) were immobilized to Affi-Gel 10 resin and went through BM cell lysates. Eluted fractions were resolved by SDS-PAGE, followed by silver staining. M, molecular weight marker. A differential band around 95 kD in CCP3-mut lane was cut for mass spectrometry. (C) Myc-tagged BAP1 and Flag-tagged CCP3-wt or CCP3-mut were cotransfected into HEK293T cells for 48 h. Cell lysates were incubated with anti-Flag antibody for immunoprecipitation assay, followed by Western blotting with anti-Myc and anti-Flag antibodies. (D) CCP3-wt and CCP3-mut were overexpressed in *Ccp3*^{-/-} LT-HSCs with pMys retrovirus. After 7-d cultures, cells were lysed and incubated with anti-CCP3 antibody, followed by immunoprecipitation and Western blotting with anti-BAP1 and anti-CCP3 antibodies. (E) LSK lysates from *Ccp3*^{+/+} and *Ccp3*^{-/-} mice were immunoprecipitated with anti-BAP1 antibody, followed by immunoblotting with GT335 antibody. (F) LSKs were incubated with RPM1640 medium and treated with CoCl₂ (10 μM) or phenanthroline (1 μM) at 37°C for 8 h. Cell lysates were incubated with anti-BAP1 antibody, followed by immunoprecipitation and Western blotting with GT335 and anti-BAP1 antibodies. Data are representative of three independent experiments. IP, immunoprecipitation.

interaction (Fig. 5 D). In parallel, BAP1 glutamylation surely promoted its UBE2O-mediated ubiquitination (Fig. 5 E). Consistently, BAP1 glutamylation only enhanced K48-linked ubiquitination, but not K63-linked ubiquitination (Fig. 5 F). More importantly, K48-linked ubiquitination of BAP1 was much more accumulated in *Ccp3*^{-/-} LSKs than in *Ccp3*^{+/+} BM LSKs (Fig. 5 G). However, BAP1 in *Bap1*^{E651A} LSKs was still stable following CHX treatment (Fig. 5 H). Altogether, BAP1 glutamylation promotes its interaction with UBE2O and accelerates K48-linked ubiquitination of BAP1 for degradation.

BAP1 facilitates *Hoxa1* expression, which is required for HSC self-renewal

We next conducted transcriptome analysis between *Ccp3*^{+/+} and *Ccp3*^{-/-} LT-HSCs through RNA sequencing. Of differential gene changes of *Ccp3*^{+/+} and *Ccp3*^{-/-} LT-HSCs, 601 genes were downregulated and 532 genes were upregulated (Fig. S4 A). Hematopoiesis and lymphocyte differentiation-related genes were downregulated (Fig. S4 B). Through gene set enrichment analysis (GSEA), HSPC-related gene sets were enriched in *Ccp3*^{+/+} LT-HSCs, whereas cell cycle-related gene sets were enriched in CCP3-deficient LT-HSCs (Fig. S4 C). Since *Ccp3*^{-/-} cells

showed reduced BAP1 protein levels, we supposed that some differential genes might overlap between *Ccp3*^{-/-} HSCs and BAP1-deficient HSCs. In fact, *Ccp3*^{-/-} HSCs displayed overlapping differential genes with BAP1-deficient LSKs (Fig. S4 C). Transcription factors (TFs) were essential to HSC function, and we found that many TFs were differentially regulated in *Ccp3*^{-/-} versus *Ccp3*^{+/+} LT-HSCs (Fig. 6 A). The top 10 downregulated TFs in *Ccp3*^{-/-} HSCs were further verified via quantitative PCR (qPCR; Fig. S4 D). We then silenced these 10 TFs in HSCs by shRNAs and followed by single-cell culture assay (Fig. S4 E). We observed that *Hoxa1* depletion most significantly impaired HSC expansion (Fig. 6 B). *Hoxa1* is a member of the homeobox (Hox) gene encoding TFs, which plays a critical role in development and tumor progression (Bach et al., 2010; Makki and Capocchi, 2010; Wang et al., 2015). Of note, we observed that only *Hoxa1* was remarkably downregulated in *Ccp3*^{-/-} LT-HSCs, while other *HoxA* genes were unchanged between *Ccp3*^{+/+} and *Ccp3*^{-/-} LT-HSCs (Fig. S4 F). We next wanted to determine how BAP1 regulated *Hoxa1* expression. Through chromatin immunoprecipitation (ChIP), we found that BAP1 accumulated onto *Hoxa1* promoter (Fig. 6 C). BAP1 overexpression in HSCs facilitated *Hoxa1* transcription, whereas overexpression of BAP1 with *Hoxa1*

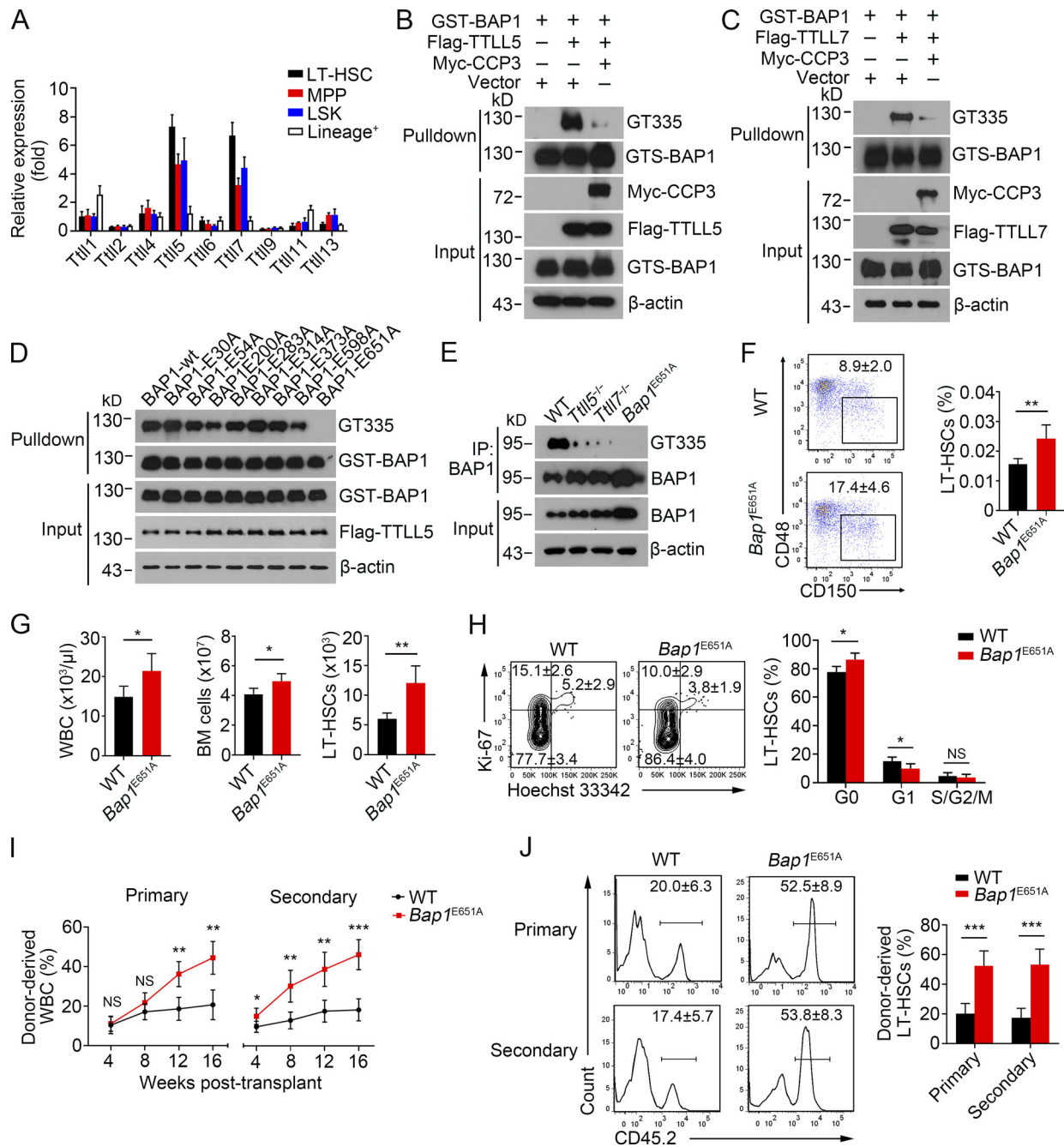


Figure 4. **BAP1 is glutamylated at Glu651 by TLL5 and TLL7.** (A) mRNA levels of *Tll* family member genes were examined in LT-HSCs, MPPs, LSKs, and lineage positive cells by real-time qPCR. Results were normalized to endogenous *Actb* gene ($n = 4$). (B and C) Flag-tagged TLL5 (B) or TLL7 (C) and Myc-tagged CCP3 were cotransfected into HEK293T cells for 48 h. Cell lysates were incubated with recombinant GST-BAP1 at 37°C for 2 h, followed by incubating with GST beads at 4°C for 1 h and immunoblotting. Protein glutamylation was tested with GT335 antibody. (D) Flag-tagged TLL5 was transfected into HEK293T cells for 48 h. Cell lysates were incubated with recombinant WT BAP1 or various indicated mutants at 37°C for 2 h, followed by incubating with GST beads at 4°C for 1 h and Western blotting for the precipitate. Protein glutamylation was examined with GT335 antibody. (E) WT, *Tll5*^{-/-}, *Tll7*^{-/-}, and *Bap1*^{E651A} LSK cell lysates were immunoprecipitated with anti-BAP1 antibody, followed by Western blotting with GT335 antibody. (F) Left: Flow cytometry analysis of LT-HSCs in WT and *Bap1*^{E651A} mice. Right: The percentage of LT-HSCs in BM cells per femur was calculated ($n = 6$). (G) Cell numbers of peripheral WBCs, BM cells, and LT-HSCs in WT and *Bap1*^{E651A} mice ($n = 6$). (H) Cell cycle analysis of WT and *Bap1*^{E651A} LT-HSCs ($n = 5$). (I and J) 1×10^2 LT-HSCs from WT and *Bap1*^{E651A} mice (CD45.2) were sorted and mixed with 5×10^5 helpers (CD45.1) and then cotransplanted into lethally irradiated (CD45.1) mice. 16 wk after transplantation, 1×10^2 LT-HSCs from donors (CD45.2) were sorted and mixed with 5×10^5 helpers (CD45.1) for secondary transplantation. Donor-derived peripheral WBCs (CD45.2) were analyzed by flow cytometry every 4 wk ($n = 5$). Donor-derived LT-HSCs (CD45.2) were analyzed by flow cytometry 16 wk after each transplantation ($n = 5$). Results are shown as means \pm SD. *, $P < 0.05$; **, $P < 0.01$; ***, $P < 0.001$. Two-tailed Student's *t* test. Data in F–H are pooled from three independent experiments. Data in A–E, I, and J are representative of three independent experiments. IP, immunoprecipitation.

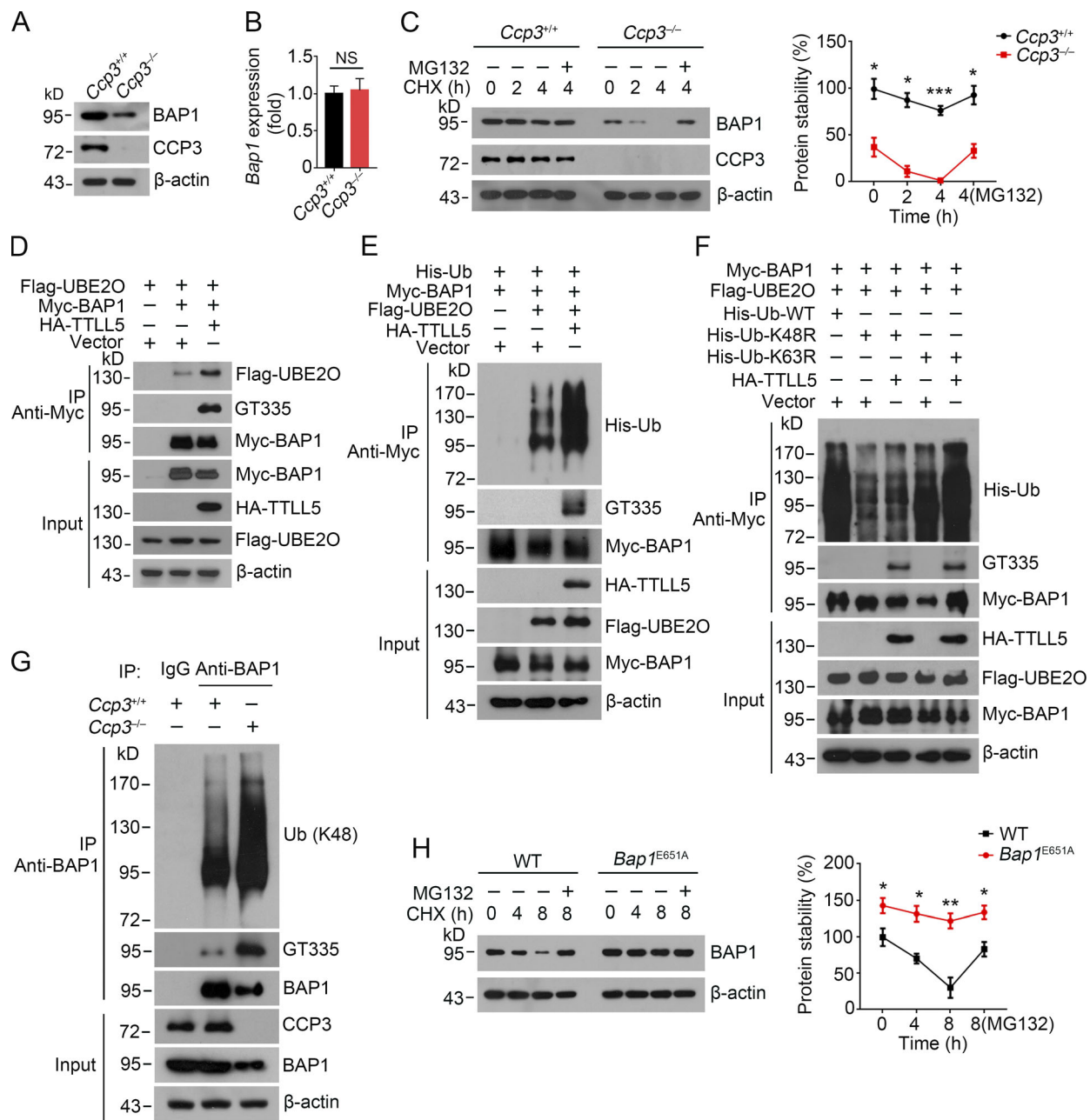


Figure 5. BAP1 glutamylation facilitates its K48-linked ubiquitination for its degradation. (A) 10^6 LSK cells sorted from *Ccp3*^{+/+} and *Ccp3*^{-/-} mice were probed by Western blotting with anti-BAP1 antibodies. (B) *Bap1* mRNA levels in *Ccp3*^{+/+} and *Ccp3*^{-/-} LSKs were detected by real-time qPCR ($n = 4$). (C) 10^6 LSKs from *Ccp3*^{+/+} and *Ccp3*^{-/-} mice were treated with CHX (20 μ g/ml) and MG132 (10 μ M). Left: At different time points, equal amounts of cells were sampled and protein levels were analyzed by Western blotting with anti-BAP1 antibody. Right: Percentages of remaining protein amounts were normalized to the initial WT cell amount and calculated as means \pm SD ($n = 3$). (D) Flag-tagged UBE20, Myc-tagged BAP1, and HA-tagged TLL5 vectors were cotransfected into HEK293T cells for 48 h. Cell lysates were incubated with anti-Myc antibody for immunoprecipitation, followed by Western blotting. (E) His-tagged ubiquitin, Myc-tagged BAP1, Flag-tagged UBE20, and HA-tagged TLL5 vectors were cotransfected into HEK293T cells for 48 h and assayed as in D. (F) Myc-tagged BAP1, Flag-tagged UBE20, HA-tagged TLL5, and His-tagged WT ubiquitin or its mutant form vectors (Ub-K48R or Ub-K63R) were cotransfected into HEK293T cells for 48 h and assayed as in D. (G) 10^6 *Ccp3*^{+/+} and *Ccp3*^{-/-} LSK cell lysates were incubated with anti-BAP1 antibody for immunoprecipitation, followed by Western blotting with K48-linked specific ubiquitination antibody or GT335 antibody. (H) 10^6 LSKs from WT and *Bap1*^{E651A} mice were treated with CHX (20 μ g/ml) and MG132 (10 μ M). Left: At indicated time points, an equal amount of cells was sampled and protein levels were analyzed by Western blotting with anti-BAP1 antibody. Percentages of remaining protein amounts were normalized to the initial WT cell amount and calculated as means \pm SD ($n = 3$). *, $P < 0.05$; **, $P < 0.01$; ***, $P < 0.001$. Two-tailed Student's *t* test. Data are representative of three independent experiments. IP, immunoprecipitation.

promoter binding region deletion had no such effect (Fig. 6 D and Fig. S4 G). By contrast, BAP1 depletion decreased *Hoxa1* expression. Additionally, BAP1 overexpression in *Ccp3*^{-/-} HSCs

rescued *Hoxa1* expression (Fig. 6 E and Fig. S4 H). Consistently, CCP3 deficiency or BAP1 depletion caused the *Hoxa1* promoter to be more resistant to DNase I digestion, and BAP1 overexpression

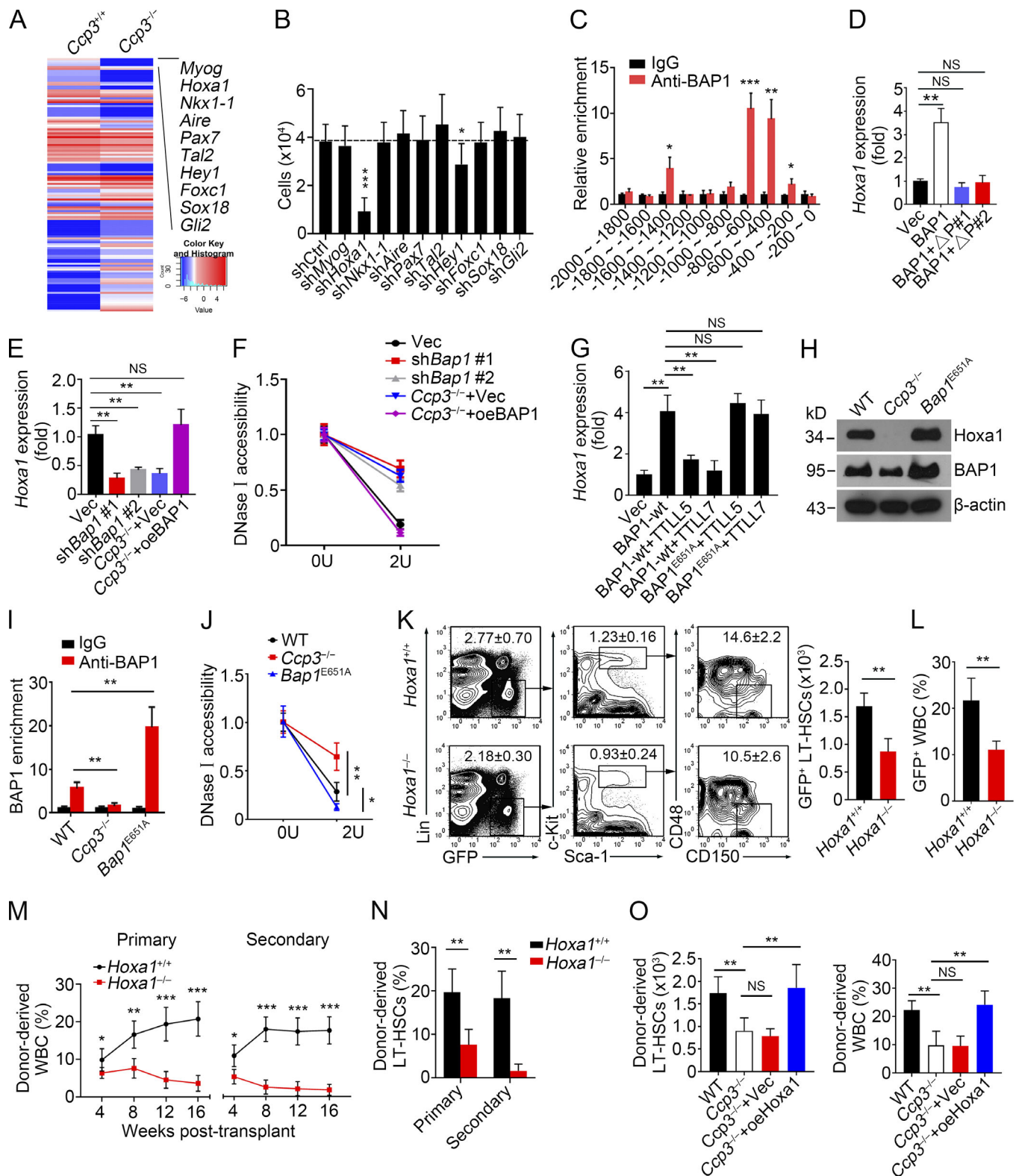


Figure 6. **BAP1 facilitates *Hoxa1* expression that is required for HSC self-renewal.** (A) Heat map of upregulated and downregulated (greater than threefold change) expression values of TFs from RNA-seq data of *Ccp3*^{+/+} and *Ccp3*^{-/-} LT-HSCs. The top 10 downregulated TFs in *Ccp3*^{-/-} LT-HSCs are shown. (B) LT-HSCs were infected with LMP retrovirus carrying respective shRNA, followed by single-cell culture. Cells were calculated 7 d later (*n* = 8). (C) Enrichment assessment of BAP1 on indicated regions of *Hoxa1* promoter in cultured HSCs. Enrichments were detected by qPCR with the indicated primers and normalized to IgG enrichment value (*n* = 4). (D) LT-HSCs were sorted and infected with lentivirus containing BAP1, Cas9, and the indicated sgRNAs, targeting the BAP1 binding region of *Hoxa1* promoter, followed by single-cell culture. 7 d later, partition of cells from each well was performed with PCR and TA clone for DNA sequencing. Cells from the corresponding wells that successfully deleted the indicated region (Δ P#1 or Δ P#2) were collected for qPCR. *Hoxa1* expression

values were normalized to endogenous *Actb* gene ($n = 5$). **(E)** LT-HSCs were infected with LMP retrovirus carrying shRNA to knock down BAP1. BAP1 was overexpressed in *Ccp3*^{-/-} LT-HSCs with pMYs retrovirus, followed by qPCR to detect *Hoxa1* expression ($n = 4$). **(F)** BAP1 was knocked down in WT LT-HSCs or overexpressed in *Ccp3*^{-/-} LT-HSCs. 10⁶ cells were lysed and nuclei were extracted for DNase I digestion. Undigested DNA was extracted and analyzed by qPCR with *Hoxa1* promoter-specific primer. Results were normalized respective to 0 U DNase I-treated samples ($n = 4$). **(G)** BAP1-wt or BAP1-mut with TLL5 or TLL7 was co-overexpressed in *Ttll5*^{-/-};*Ttll7*^{-/-} LT-HSCs with pMYs retrovirus, followed by qPCR to detect *Hoxa1* expression ($n = 4$). **(H)** WT, *Ccp3*^{-/-}, and *Bap1*^{E651A} LSKs were probed by Western blotting with the indicated antibodies. **(I)** Enrichment assessment of BAP1 on the BAP1 binding region of *Hoxa1* promoter in WT, *Ccp3*^{-/-}, and *Bap1*^{E651A} LSKs, followed by qPCR, and values normalized to IgG enrichment value ($n = 4$). **(J)** 10⁶ WT, *Ccp3*^{-/-}, and *Bap1*^{E651A} LSKs were lysed for nuclear extraction and DNase I digestion. Remaining DNA was extracted and analyzed by qPCR with *Hoxa1* promoter-specific primer. Results were normalized respective to 0 U DNase I-treated samples ($n = 4$). **(K and L)** *Hoxa1* was knocked out in LT-HSCs from Cas9 knock-in mice through infection of lentivirus carrying Cre and indicated sgRNA, and then 1 × 10² GFP⁺ LT-HSCs were sorted and cotransplanted with 5 × 10⁵ helpers (CD45.1) into lethally irradiated CD45.1 mice. 16 wk after BM transplantation, LT-HSCs were detected by flow cytometry (left), and absolute *Hoxa1*^{+/+} and *Hoxa1*^{-/-} LT-HSCs were calculated (right). $n = 6$. **(M and N)** 1 × 10² GFP⁺ *Hoxa1*^{+/+} and *Hoxa1*^{-/-} LT-HSCs were sorted and cotransplanted with 5 × 10⁵ helpers (CD45.1) into lethally irradiated CD45.1 mice. 16 wk after transplantation, 1 × 10² GFP⁺ LT-HSCs were sorted for secondary LT-HSC transplantation. GFP⁺ peripheral WBCs were analyzed by flow cytometry every 4 wk (M), and GFP⁺ LT-HSCs were analyzed 16 wk after primary and secondary transplantation (N). $n = 6$. **(O)** *Hoxa1* was overexpressed with pMYs retrovirus into *Ccp3*^{-/-} LT-HSCs, and GFP⁺ cells were sorted. 1 × 10² *Ccp3*^{+/+} and *Ccp3*^{-/-} LT-HSCs and *Hoxa1*-overexpressing *Ccp3*^{-/-} LT-HSCs (CD45.2) were cotransplanted with 5 × 10⁵ helpers (CD45.1) into lethally irradiated CD45.1 mice. 16 wk after BM transplantation, LT-HSCs (left) and WBCs (right) from engrafted recipient mice were analyzed by flow cytometry ($n = 6$). Results are shown as means ± SD. *, $P < 0.05$; **, $P < 0.01$; ***, $P < 0.001$. Two-tailed Student's *t* test. Data in B–O are representative of three independent experiments.

in *Ccp3*^{-/-} HSCs made the *Hoxa1* promoter more accessible (Fig. 6 F). These data suggest that BAP1 accumulates on the *Hoxa1* promoter and facilitates *Hoxa1* expression.

As a nuclear deubiquitylase, BAP1 can remove monoubiquitin from histone H2A lysine 119 (H2AK119), playing a critical role in regulating gene expression (Balasubramani et al., 2015). We then measured H2AK119Ub and H3K27me3 on *Hoxa1* promoter in *Ccp3*^{-/-} LSKs. We found elevated enrichment of H2AK119Ub and H3K27me3 on the *Hoxa1* promoter in *Ccp3*^{-/-} LSKs (Fig. S4, I and J). These data suggest that BAP1 could indirectly regulate *Hoxa1* expression through effects on H2AK119Ub and other chromatin marks in HSCs.

We next generated *Ttll5* and *Ttll7* double knockout (DKO) mice (*Ttll5*^{-/-};*Ttll7*^{-/-}). We found that BAP1-wt overexpression in *Ttll5*^{-/-};*Ttll7*^{-/-} HSCs could promote *Hoxa1* expression (Fig. 6 G and Fig. S4 K). However, co-overexpression of BAP1-wt with TLL5 or TLL7 in *Ttll5*^{-/-};*Ttll7*^{-/-} HSCs suppressed this transcription-promoting effect. By contrast, overexpression of BAP1^{E651A} plus TLL5 or TLL7 in *Ttll5*^{-/-};*Ttll7*^{-/-} HSCs restored *Hoxa1* transcription (Fig. 6 G and Fig. S4 K). These data suggest that BAP1 glutamylation suppresses *Hoxa1* transcription. In addition, *Hoxa1* was dramatically decreased in *Ccp3*^{-/-} HSCs, whereas it was increased in *Bap1*^{E651A} HSCs (Fig. 6 H). Parallely, BAP1 was not deposited on *Hoxa1* promoter in *Ccp3*^{-/-} HSCs, while it was enriched on the promoter region in *Bap1*^{E651A} HSCs (Fig. 6 I). Accordingly, BAP1-E651A caused *Hoxa1* promoter to be more accessible to DNase I digestion, indicating the open state of the *Hoxa1* promoter (Fig. 6 J). These data indicate that BAP1 glutamylation causes its degradation to suppress *Hoxa1* expression.

We next generated *Hoxa1*^{-/-} LT-HSCs via Cas9 knock-in mice as previously described (Platt et al., 2014; Fig. S4 L), followed by BM transplantation assay. We observed that engraftment of *Hoxa1*^{-/-} LT-HSCs generated reduced numbers of LT-HSCs and peripheral blood cells (Fig. 6, K and L). Of note, *Hoxa1*^{-/-} LT-HSCs could not sustain their quiescence, similar to *Ccp3*^{-/-} LT-HSCs (Fig. S4 M). However, *Hoxa1*^{-/-} LT-HSCs did not undergo apparent apoptosis (Fig. S4 N). Through serial LT-HSC transplantation, *Hoxa1*^{-/-} LT-HSCs failed to reconstitute peripheral

blood cells and could not maintain their self-renewal (Fig. 6, M and N). Transplantation of *Hoxa1*-overexpressing *Ccp3*^{-/-} LT-HSCs could restore the normal numbers of HSCs and peripheral blood cells compared with engraftment of WT LT-HSCs (Fig. 6 O and Fig. S4 O). These results indicate that *Hoxa1* is required for the maintenance of HSC self-renewal.

TLL5 and TLL7 deficiencies sustain BAP1 stability to promote HSC self-renewal and hematopoiesis

Given that BAP1 glutamylation was catalyzed by TLL5 and TLL7, we next tested how *Ttll5* and *Ttll7* deficiencies affected hematopoietic phenotypes. We observed that *Ttll5*- and *Ttll7*-deficient mice displayed higher numbers and percentages of LSKs and LT-HSCs compared with their WT littermate control mice (Fig. 7 A and Fig. S5 A). Moreover, *Ttll5* and *Ttll7* DKO mice showed much higher numbers of LSKs and LT-HSCs compared with *Ttll5*- or *Ttll7*-deficient mice alone (Fig. 7 A). As expected, *Ttll5*^{-/-} or *Ttll7*^{-/-} LSKs showed much less glutamylation of BAP1 and much higher protein levels of BAP1 compared with WT control mice (Fig. 7 B). In addition, *Hoxa1* was highly expressed in *Ttll5*^{-/-} and *Ttll7*^{-/-} HSCs (Fig. 7, B and C). Consequently, *Ttll5*- and *Ttll7*-deficient mice had higher numbers of BM and peripheral blood cells than WT mice (Fig. 7 D and Fig. S5 B). In addition, through in vitro replating clone formation assay, *Ttll5*^{-/-} and *Ttll7*^{-/-} LT-HSCs showed stronger expansion capacities, and DKO LT-HSCs showed much stronger expansion capacity than *Ttll5*^{-/-} or *Ttll7*^{-/-} mice alone (Fig. 7 E). Through BM transplantation, engraftment of *Ttll5*^{-/-} and *Ttll7*^{-/-} LT-HSCs displayed increased numbers of LT-HSCs and peripheral blood cells (Fig. 7, F and G). Finally, *Ttll5*^{-/-} and *Ttll7*^{-/-} LT-HSCs kept quiescent similar to *Bap1*^{E651A} LT-HSCs (Fig. 7 H). Collectively, TLL5 and TLL7 deficiencies promote HSC self-renewal and hematopoiesis.

Discussion

HSCs maintain self-renewal with a sophisticated mechanism to provide lifelong hematopoiesis. However, the mechanism underlying HSC self-renewal is still elusive. In this study, we

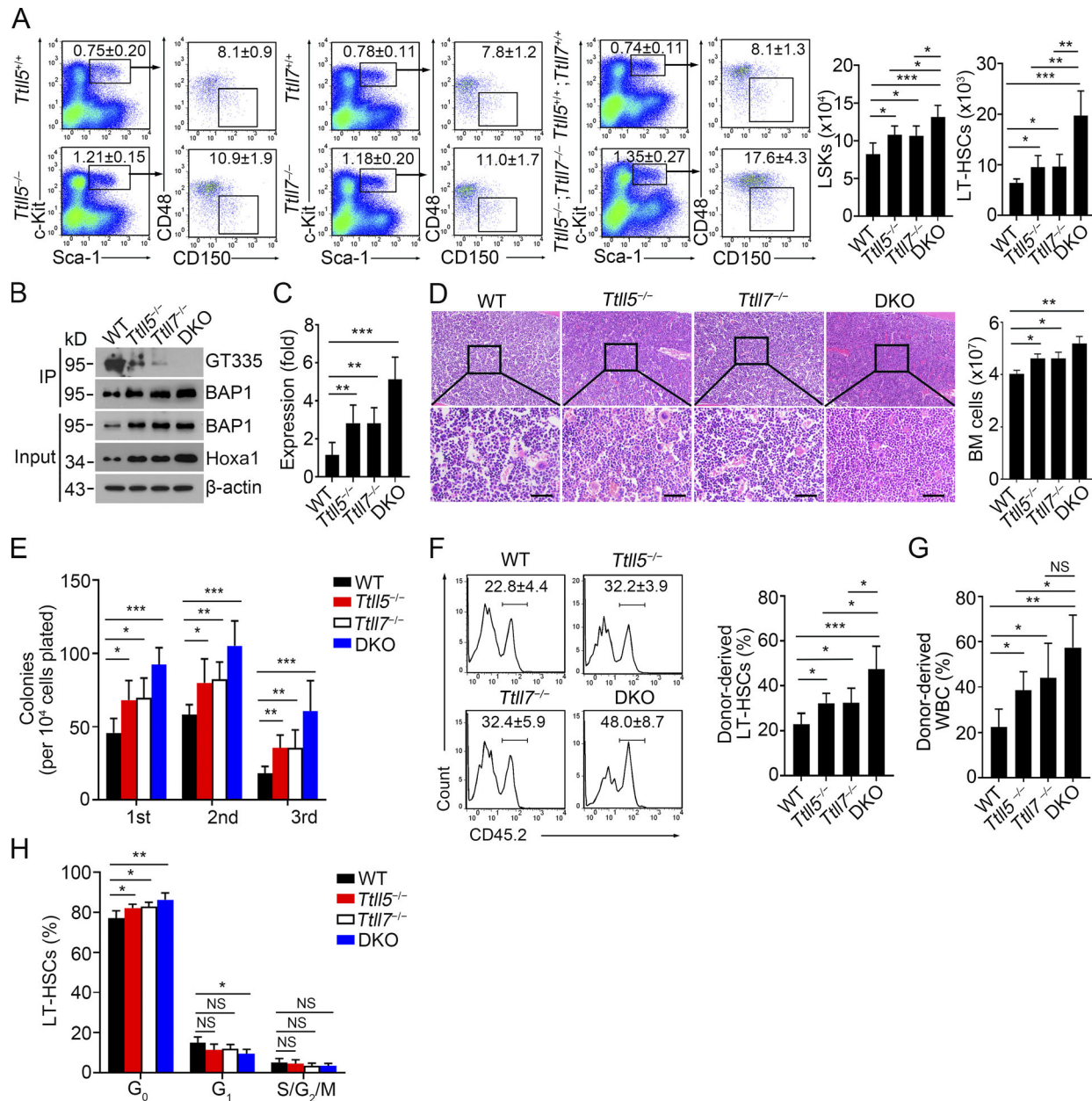


Figure 7. *Ttl5* and *Ttl7* deficiencies promote *Hoxa1* expression and HSC self-renewal. (A) LSKs and LT-HSCs from WT, *Ttl5*^{-/-}, *Ttl7*^{-/-}, and *Ttl5*^{-/-}; *Ttl7*^{-/-} (DKO) mice were detected by flow cytometry (left), and absolute numbers were calculated (right). *n* = 6. (B) WT, *Ttl5*^{-/-}, *Ttl7*^{-/-}, and DKO LSKs were sorted and lysated, and then immunoprecipitated with anti-BAP1 antibody, followed by Western blotting with GT335 and anti-*Hoxa1* antibodies. (C) LT-HSCs from WT, *Ttl5*^{-/-}, *Ttl7*^{-/-}, and DKO mice were sorted, followed by qPCR to analyze *Hoxa1* expression (*n* = 6). (D) H&E staining of BM sections from femurs of WT, *Ttl5*^{-/-}, *Ttl7*^{-/-}, and DKO mice (left), and absolute BM cell numbers (right). *n* = 6. Scale bars, 50 μ m. (E) Serial CFU assay of WT, *Ttl5*^{-/-}, *Ttl7*^{-/-}, and DKO BM cells. 1×10^4 BM cells were plated in M3434 and serially replated every 7 d (*n* = 6). (F and G) 1×10^2 WT, *Ttl5*^{-/-}, *Ttl7*^{-/-}, and DKO LT-HSCs were cotransplanted with 5×10^5 helpers (CD45.1) into lethally irradiated CD45.1 mice. (F) 16 wk after BM transplantation, engrafted LT-HSCs were analyzed by flow cytometry and calculated. (G) Percentages of donor-derived (CD45.2⁺) WBCs were calculated (*n* = 5). (H) Cell cycle analysis of WT, *Ttl5*^{-/-}, *Ttl7*^{-/-}, and DKO LT-HSCs (*n* = 5). Results are shown as means \pm SD. *, *P* < 0.05; **, *P* < 0.01; ***, *P* < 0.001. Two-tailed Student's *t* test. Data in A and D are pooled from three independent experiments. Data in B, C, and E–H are representative of three independent experiments. IP, immunoprecipitation.

showed that CCP3 is most highly expressed in BM cells among CCP members. CCP3 deficiency impairs HSC self-renewal and hematopoiesis. BAP1 is a substrate for CCP3 in LT-HSCs. BAP1 is catalyzed at Glu651 by TTLL5 and TTLL7, and BAP1-E651A mutation abrogates BAP1 glutamylation. BAP1 glutamylation accelerates its ubiquitination to trigger its degradation. CCP3 can remove glutamylation of BAP1 to promote its stability, which

enhances *Hoxa1* expression leading to HSC self-renewal. *Bap1*^{E651A} mice produce higher numbers of LT-HSCs and peripheral blood cells, and *Bap1*^{E651A} LT-HSCs were more quiescent. Moreover, TTLL5 and TTLL7 deficiencies sustain BAP1 stability to promote HSC self-renewal and hematopoiesis (Fig. S5 C).

Protein glutamylation is catalyzed by a family of polyglutamylases, also called TTLLs (Janke et al., 2005). The

well-known substrates of glutamylation are tubulins. Tubulins are glutamylated at their acidic, glutamate-rich C termini, which are the binding sites for most microtubule (MT)-associated proteins (Janke and Bulinski, 2011). Thus, tubulin glutamylation generates functionally divergent MTs by regulating the affinity between MT-associated proteins and MTs (van Dijk et al., 2008). Through regulating MT character, glutamylation is therefore proposed to be involved in MT-related cellular processes, including stability of centrosomes, motility of cilia and flagella, and neurite outgrowth, as well as neurodegeneration (Bosch Grau et al., 2013; Rogowski et al., 2010). Given that TLLs have different expression patterns in diverse tissues and show nonredundant functions, more novel substrates of glutamylation need to be defined. We recently reported that TLL4 and TLL6 are highly expressed in megakaryocytes and catalyze glutamylation of Mad2 to modulate megakaryocyte maturation (Ye et al., 2014). IL-7R α can be catalyzed by TLL4 and TLL13, and IL-7R α glutamylation initiates TF Sall3 expression in common helper-like innate lymphoid progenitors, leading to development of ILC3 cells (Liu et al., 2017a). In this study, we demonstrated that TLL5 and TLL7 are most highly expressed in HSCs and catalyze BAP1 glutamylation to facilitate its ubiquitylation for degradation, which regulates HSC self-renewal and hematopoiesis.

Protein glutamylation is also a reversible modification, whose glutamylation is removed by a family of carboxypeptidases, also called CCPs (Janke et al., 2005). It has been reported that CCP family members catalyze deglutamylation of tubulins and display enzymatic specificities (Rogowski et al., 2010). We previously showed that CCP6 hydrolyzes Mad2 glutamylation to modulate megakaryocyte maturation (Ye et al., 2014). We also reported that CCP2 is highly expressed in common helper-like innate lymphoid progenitors, the progenitor of ILCs, and catalyzes IL-7R α deglutamylation, leading to ILC3 development (Liu et al., 2017a). We recently demonstrated that cGAS can be glutamylated by TLL4 and TLL6, whose glutamylation can be hydrolyzed by CCP5 and CCP6 (Xia et al., 2016). Glutamylation and deglutamylation of cGAS tightly regulate immune responses to DNA virus infections. Herein, we showed that CCP3 is most highly expressed in BM cells and hydrolyzes BAP1 glutamylation to modulate HSC self-renewal and hematopoiesis. These findings suggest that different tissue and cell type distributions of TLLs and CCPs exert unique roles in the regulation of different physiological processes.

BAP1 is a member of the ubiquitin C-terminal hydrolase subfamily of deubiquitylating enzymes, which is associated with multiprotein complexes to regulate various cellular processes (Carbone et al., 2013). BAP1 mutations are implicated in various malignancies, including myeloid transformation (Abdel-Wahab and Dey, 2013). BAP1 catalytic mutation has been identified in myelodysplastic syndrome patients (Carbone et al., 2013). In addition, BAP1-deficient mice also manifest myeloid transformation (Dey et al., 2012). It has been reported that BAP1 locates at the nucleus and interacts with TFs or multiprotein complexes to regulate transcription initiation and elongation (Carbone et al., 2013; Yu et al., 2010). However, how BAP1 regulates HSC self-renewal and hematopoiesis is still unknown. In

actuality, we found elevated enrichment of H2AK119Ub and H3K27me3 on the *Hoxa1* promoter in *Ccp3*^{-/-} LSKs, suggesting that BAP1 could indirectly regulate *Hoxa1* expression through effects on H2AK119Ub and other chromatin marks in HSCs. We are still exploring the molecular mechanism by which BAP1 glutamylation modulates *Hoxa1* expression in a direct or indirect manner in HSCs. TLL5- and TLL7-mediated BAP1 glutamylation promotes its interaction with ubiquitin-conjugating enzyme UBE2O to facilitate K48-linked ubiquitination for its degradation. TLL5 and TLL7 deficiencies maintain BAP1 stability, and stable BAP1 further promotes *Hoxa1* expression, leading to enhancement of HSC self-renewal and hematopoiesis. As expected, *Hoxa1* deletion causes reduced numbers of LT-HSCs and peripheral blood cells. In summary, glutamylation and deglutamylation of BAP1 play a critical role in the regulation of HSC self-renewal and hematopoiesis.

Materials and methods

Antibodies and reagents

The following commercial antibodies were used: mouse hematopoietic lineage eFlour 450 cocktail (eBioscience; 22-7775), PerCP-Cy5.5-anti-CD45.1 (eBioscience; 45-0453), FITC-anti-CD45.2 (eBioscience; 11-0454), FITC-anti-IL-7R α (eBioscience; 11-1271), APC-anti-Ly6A/E (Sca-1, eBioscience; 17-5981), PE-anti-CD117 (c-Kit, eBioscience; 12-1171), PE-Cy7-anti-CD16/32 (eBioscience; 25-0161), APC-eFlour 780-anti-CD48 (eBioscience; 47-0481), PE-CY7-anti-CD150 (eBioscience; 25-1502), eFlour 450-anti-CD3 (eBioscience; 48-0031), PE-anti-CD19 (eBioscience; 12-0193), FITC-anti-Gr-1 (eBioscience; 11-5931), Alexa Fluor 700-anti-CD34 (eBioscience; 56-0341), FITC-anti-Ki-67 (eBioscience; 7B11), and FITC-anti-Annexin V (eBioscience; VAA-33). Anti-CCP3 (16990-1-AP) antibody was purchased from Proteintech. Anti-CCP4 (T-17), anti-GST (6G9C6), anti-Myc (9E10), anti-Flag (M1), anti- β -actin (SP124), and anti-His (6AT18) antibodies were bought from Sigma-Aldrich. GT335 antibody was obtained from AdipoGen. BAP1 (D1W9B), K48 linkage-specific polyubiquitin (D9D5), ubiquityl-histone H2A (Lys119; D27C4), and tri-methyl-histone H3 (Lys27; C36B11) antibodies were purchased from Cell Signaling Technology. TLL5 (ARP75440_PO50) antibody was obtained from Aviva Systems Biology. TLL7 (N1N2) antibody was bought from GeneTex. *Hoxa1* (BA3730-2) antibody was bought from Boster Biological Technology. Paraformaldehyde, CHX, MG132, phenanthroline, 5-FU, and DAPI were purchased from Sigma-Aldrich. CoCl₂ was from Sinopharm Chemical Reagent. EDTA-free protease inhibitor cocktail and DNase I were purchased from Roche Molecular Biochemicals. West Pico and West Femto plus chemiluminescent substrate were purchased from SageBrightness.

Generation of knockout and *Bap1*^{E651A} knock-in mice by CRISPR-Cas9 technology

Ccp1- and *Ccp6*-deficient mice were described previously (Ye et al., 2014). *Ccp2*-, *Ccp3*-, *Ccp4*-, and *Ccp5*-deficient mice were generated using CRISPR-Cas9 approaches as described (Xia et al., 2016). For generation of *Tll5*- and *Tll7*-deficient mice, vector pST1374-NLS-flag-linker-Cas9 (Addgene plasmid #44758)

expressing Cas9 and pUC57-sgRNA (Addgene plasmid #51132) expressing small guide RNAs (sgRNAs) targeting *Ttll5* and *Ttll7* genes were constructed (Table S2). Mixtures of Cas9 mRNA (100 ng/ μ l) and sgRNA (50 ng/ μ l) were microinjected into the cytoplasm of C57BL/6 fertilized eggs, followed by transfer to the uterus of pseudo-pregnant ICR-background female mice, from which viable founder mice were obtained. Genotyping of KO mice with indicated primers (Table S3) was performed as previously described (Zhu et al., 2014). We chose frameshift mutation by PCR screening and TA clone for sequencing and then confirmed knockout efficiency by Western blot. For generation of *Bap1*^{E651A} mice, the genome locus of *Bap1* gene was knocked in with BAP1-E651A mutation via a CRISPR-Cas9 approach (Ye et al., 2018). A mixture of Cas9 mRNA, sgRNA, and BAP1-E651A donor templates was microinjected into the cytoplasm of C57BL/6 fertilized eggs and transferred into the uterus of pseudo-pregnant ICR females. BAP1-E651A mutants were identified by PCR screening and TA clone for DNA sequencing. The gRNA sequence for *Bap1*^{E651A} mice was up, 5'-GCCCTAAGGTA TACAATGT-3'; down, 5'-CAGTGTCCITGGGCAGTAG-3'. Gt(ROSA)26Sor^{tm1(CAG-xstpx-cas9,-EGFP)}Fezh mice were purchased from The Jackson Laboratory (Platt et al., 2014). For deletion of *Hoxa1*, LT-HSCs from Gt(ROSA)26Sor^{tm1(CAG-xstpx-cas9,-EGFP)}Fezh knock-in mice were sorted and infected with lentivirus containing the indicated sgRNA and Cre recombinase expression. Then infected LT-HSCs were mixed with 5×10^5 helper cells and transplanted into lethally irradiated recipient mice (CD45.1). 1 mo later, GFP⁺ BM cells were sorted from the recipient mice to confirm *Hoxa1* deficiency with Western blot. GFP⁺ LT-HSCs were sorted for further transplantation. All the mice we used were C57BL/6 background and ~3 mo old. We used littermates with the same age and gender for each group. We performed three independent experiments of each mouse from at least three mice for each group. Animal use and protocols were approved by the Institutional Animal Care and Use Committees at the Institute of Biophysics, Chinese Academy of Sciences.

Histology analysis

Mouse spleens were fixed in 4% paraformaldehyde for 12 h at room temperature. Mouse femurs were fixed in PBS buffer containing 10% formaldehyde for 12 h and then decalcified in decalcifying buffer (10% EDTA in PBS, pH 7.4) for 48 h, changing new decalcifying buffer every 24 h. Fixed tissues were washed twice using 70% ethanol and embedded in paraffin, followed by sectioning and staining with H&E according to standard laboratory procedures.

Flow cytometry

BM cells were flushed out from femurs with precooled PBS buffer containing 2% FBS and sifted through 50- μ m cell strainers. RBCs were removed by suspending cells in RBC lysis buffer, followed by washing twice with PBS. BM cells were counted with a blood counting chamber at least three times and then checked again through flow cytometry with a FACSARIA III instrument (BD Biosciences). For hematopoietic lineage analysis, 10^7 BM cells were incubated with fluorophore-conjugated

antibodies at 4°C for 1 h and then washed twice. LSKs (Lin⁻Sca-1⁺c-Kit⁺), LT-HSCs (Lin⁻Sca-1⁺c-Kit⁺CD48⁻CD150⁺), short-term HSCs (Lin⁻Sca-1⁺c-Kit⁺CD48⁻CD150⁻), MPPs (Lin⁻Sca-1⁺c-Kit⁺CD48⁺CD150⁻), HSPCs (Lin⁻Sca-1⁻c-Kit⁺), CMPs (Lin⁻Sca-1⁻c-Kit⁺CD34⁺CD16/32⁻), and CLPs (Lin⁻CD127⁺Sca-1^{low}c-Kit^{low}) were analyzed or sorted with a FACSARIA III instrument. Lineage cocktail antibodies contained anti-B220, anti-CD3, anti-Ter119, anti-Gr-1, anti-CD11b, anti-CD19, and anti-NK1.1. For peripheral WBC flow cytometric analysis, blood samples were collected through tail veins, and 10 μ l of blood was incubated with 200 μ l RBC lysis buffer at room temperature for 2 min, followed by washing with PBS twice. T cells (CD3⁺), B cells (CD19⁺), and myeloid cells (CD11b⁺Gr-1⁺) were analyzed with a FACSARIA III instrument. Data were analyzed using the FlowJo 7.6.1 software.

In vitro colony-forming assay

4×10^4 BM cells from WT or KO mice were mixed with cytokine-supplemented methylcellulose medium (Methocult, M3434; STEMCELL Technologies) and plated in 35-mm tissue-culture dishes. After 10 d of culture at 37°C in 5% CO₂, granulocyte colonies, macrophage colonies, granulocyte-macrophage colonies, granulocyte, erythroid, macrophage, and megakaryocyte colonies, erythroid colonies, and megakaryocyte colonies were observed with an inverted microscope and assigned scores (Hou et al., 2015). For continuous replating colony-forming assay, 1×10^4 BM cells were initially plated in M3434 medium. Colonies were scored after 7-d cultures, and cells were resuspended and washed with PBS. Then, 1×10^4 cells were cultured again for a second or third replating (Moran-Crusio et al., 2011).

BM transplantation

BM cells from the indicated mice (CD45.2) were flushed out from femurs with precooled PBS buffer and sifted through 70- μ m cell strainers. 1×10^6 BM cells were then transplanted into lethally irradiated (10 Gy) recipient mice (CD45.1) through tail veins. The indicated parameters were detected 16 wk after BM transplantation. For LT-HSC transplantation, 1×10^2 LT-HSCs were sorted and mixed with 5×10^5 BM helpers (CD45.1) and then transplanted into lethally irradiated recipient mice (CD45.1), followed by examination at the times mentioned. For competitive BM transplantation, 1×10^6 BM (CD45.2) cells were mixed with 1×10^6 BM competitors (CD45.1) to be transplanted into lethally irradiated recipient mice (CD45.1⁺CD45.2⁺). Peripheral WBCs were detected every 4 wk. LT-HSCs from different donors were identified with anti-CD45.1 and anti-CD45.2 antibodies through flow cytometry 16 wk after transplantation.

In vitro single LT-HSC culture assay

In vitro single LT-HSC culture assay was performed as described previously (Rathinam et al., 2011). In brief, we isolated LT-HSCs (Lin⁻Sca-1⁺c-Kit⁺CD48⁻CD150⁺) by flow cytometry and sorted single cells into 96-well plates. Single LT-HSCs were cultured in vitro in the presence of the following recombinant cytokines: mouse stem cell factor (50 ng/ml), mouse thrombopoietin (10 ng/ml), mouse IL-3 (10 ng/ml), mouse IL-6 (10 ng/ml), and human Flt3L (50 ng/ml; all from Peprotech). Cells were cultured in IMDM supplemented with 10% (volume/volume) FCS, 2 mM

L-glutamine, 1% (volume/volume) penicillin-streptomycin, and 1 mM nonessential amino acids. 3 d later, cells were transferred into 24-well plates with 1 ml fresh medium containing cytokines for further culture. After 7-d cultures, cells were counted with a blood counting chamber or analyzed by flow cytometry.

Western blot

10^6 sorted LSKs or cultured HSCs were lysed with RIPA buffer (150 mM NaCl, 0.5% sodium deoxycholate, 0.1% SDS, 1% NP-40, 1 mM EDTA, and 50 mM Tris, pH 8.0, containing protease inhibitor cocktail) at 4°C for 30 min, followed by separation with SDS-PAGE. Samples were then transferred onto nitrocellulose membranes and incubated with primary antibodies in 5% BSA at room temperature for 2 h. After washing with Tris-buffered saline containing 0.1% Tween-20 three times, membranes were incubated with HRP-conjugated secondary antibodies at room temperature for 1 h. Chemiluminescent signals were generated using West Pico or West Femto plus enhanced chemiluminescent substrate.

Immunoprecipitation assay

HEK293T cells were transfected with the indicated plasmids and cultured for 48 h. For endogenous immunoprecipitation, 1×10^6 LSKs were sorted or LT-HSCs were cultured for expansion. Cells were lysed with radioimmunoprecipitation assay buffer at 4°C for 1 h. Lysates were incubated with the indicated antibodies for 2 h and immunoprecipitated with protein A/G agarose beads for 1 h, followed by SDS-PAGE separation and immunoblotting.

Quantitative real-time PCR

Cell populations were isolated by flow cytometry. Total RNAs were extracted with RNA Miniprep Kit (Tiangen Biotech) according to the manufacturer's protocol. Then, cDNA was synthesized with M-MLV reverse transcription (Promega). mRNA transcripts were analyzed with the ABI 7300 qPCR system using specific primer pairs as listed in Table S3. Relative expressions were calculated and normalized to endogenous *Actb* expression.

Recombinant protein expression

cDNAs were cloned from a BM cDNA library. CCP3-wt, CCP3-mut, BAP1-wt, and indicated BAP1 mutants were cloned into pGEX6p-1 plasmid for GST-tagged protein expression. Plasmids were transformed into *Escherichia coli* strain BL21 (DE3), followed by induction with 0.1 mM isopropyl β -D-1-thiogalactopyranoside at 16°C for 24 h. Cells were collected and lysed by an ultrasonic cell disruption system (Branson), followed by purification with GST resins.

ChIP assay

ChIP assay was described previously (Liu et al., 2017b). In brief, 1×10^6 LSKs or cultured HSCs were cross-linked with 1% formaldehyde at 37°C for 10 min. Then, cells were washed twice with PBS, lysed, and sonicated to get 300–500-bp DNA fragments. Lysates were incubated with 4 μ g anti-BAP1 antibody rolling overnight at 4°C. Salmon sperm DNA/protein agarose beads were added for DNA immunoprecipitation. After washing, DNA was eluted from beads and purified. DNA fragments were

extracted and analyzed with qPCR. Primers used for ChIP are listed in Table S4.

RNA interference and gene overexpression

Target sequences for RNA interference were designed according to MSCV-LTRmiR30-PIG (LMP) system instructions. LMP vectors containing target sequences were constructed. shRNA sequences are listed in Table S5. For gene overexpression, the indicated genes were cloned into pMYs-IRES-GFP (pMYs) retrovirus vectors. LMP or pMYs vectors were cotransfected with packaging plasmid PCL122 into HEK293T cells for 48 h. Media containing virus particles were collected and ultracentrifuged at 25,000 rpm (82,700 g) for 2 h for viral concentration. Pellets were resuspended in IMDM, and viral titers were determined by infecting HEK293T cells with diluted viruses. LT-HSCs were sorted and incubated with viruses in the presence of 8 μ g/ml polybrene, followed by centrifuging at 500 g for 2 h. After 36-h culture to allow gene expression, GFP⁺ cells were sorted for transplantation or further cultured for another 2 d to get enough cells for analyzing gene expression or other experiments as mentioned.

DNase I accessibility assay

DNase I digestion assay was performed as described previously (Liu et al., 2017a). In brief, nuclei were purified from 1×10^6 LSKs or cultured HSCs, according to the manufacturer's protocol, with the Nuclei Isolation Kit (Sigma-Aldrich). Then, nuclei were resuspended with DNase I digestion buffer and treated with indicated units of DNase I (Sigma-Aldrich) at 37°C for 5 min. 2 \times DNase I stop buffer (20 mM Tris, pH 8.0, 4 mM EDTA, and 2 mM EGTA) was added to stop reactions. DNA was extracted and examined by qPCR.

In vitro glutamylation assay

Detailed protocol for in vitro glutamylation assay was previously described (Ye et al., 2014). In brief, CCP3, TTLL5, and TTLL7 were transfected into HEK293T cells for 48 h. Cells were harvested and lysed. Supernatants were incubated with GST-BAP1 or indicated mutants at 37°C for 2 h. GST-BAP1 was precipitated, followed by immunoblotting to detect glutamylation with GT335 antibody.

Gene expression analysis

10^4 LT-HSCs (Lin⁻Sca-1⁺c-Kit⁺CD48⁻CD150⁺) from *Ccp3*^{+/+} and *Ccp3*^{-/-} mice were sorted by flow cytometry. Total RNA was extracted with the RNA Miniprep Kit and was qualified using Agilent 2100 for the construction of sequencing libraries. Libraries were sequenced on BGISEQ-500 using 50-bp single-end reads. Heatmap.2, ggplot2, and clusterProfiler in Bioconductor were used for generating heatmap, volcano plot, and gene ontology analyzing. GSEA v4.0.1 was used. RNA-seq data have been deposited under GEO accession no. GSE138298.

Statistical analysis

For statistical analysis, data were analyzed by Sigma Plot or GraphPad Prism 5.0. Two-tailed unpaired Student's *t* test was used in this study. P values < 0.05 were considered significant

(*, $P < 0.05$; **, $P < 0.01$; ***, $P < 0.001$); P values > 0.05 were considered nonsignificant. All flow cytometry data were analyzed with FlowJo (Treestar).

Online supplemental materials

Fig. S1 shows that *Ccp3* deletion impairs HSC expansion. Fig. S2 shows that CCP3 plays an intrinsic role in HSC self-renewal. Fig. S3 shows that BAP1 is glutamylated at E651 by TLL5 and TLL7. Fig. S4 shows that BAP1 targets the *Hoxa1* promoter to enhance *Hoxa1* expression. Fig. S5 shows that *Ttll5* and *Ttll7* deficiencies promote HSC self-renewal. Table S1 shows hematopoietic cell counts in peripheral blood of *Ccp3*^{+/+} and *Ccp3*^{-/-} mice. Table S2 shows sgRNA sequences used in this study. Table S3 shows sequences of primers used for genotyping and qPCR. Table S4 shows sequences of primers used in ChIP assays. Table S5 shows sequences for shRNAs used in this study.

Acknowledgments

We thank Peng Xue, Jianhua Wang, Di Liu, Yan Teng, Junying Jia, Shu Meng, Jing Cheng, Yihui Xu, Xudong Zhao, and Jianhui Li for technical support. We thank Xiang Shi and Xing Gao for animal procedures. We thank Zhimin Wang and the HPC Service Station for data analysis.

This work was supported by the National Natural Science Foundation of China (31930036, 81921003, 31530093, 91640203, 31871494, 31671531, 31670886, 81601361, 31570872, 31728006, 81572433, 81772646, 31601189); the Strategic Priority Research Programs of the Chinese Academy of Sciences (XDB19030203, XDA12020219); and the Beijing Natural Science Foundation (7181006).

Author contributions: Z. Xiong designed and performed experiments, analyzed data, and wrote the paper. P. Xia performed experiments and analyzed data. X. Zhu generated genetic mice. J. Geng, S. Wang, B. Ye, and X. Qin performed some experiments. Y. Qu, L. He, and D. Fan crossed and genotyped some mice. Y. Du analyzed some data. Y. Tian initiated the study and built up animal models; Z. Fan initiated the study, organized, designed, and wrote the paper.

The authors declare no competing financial interests.

Submitted: 1 June 2019

Revised: 27 August 2019

Accepted: 9 October 2019

References

Abdel-Wahab, O., and A. Dey. 2013. The ASXL-BAP1 axis: new factors in myelopoiesis, cancer and epigenetics. *Leukemia*. 27:10–15. <https://doi.org/10.1038/leu.2012.288>

Bach, C., S. Buhl, D. Mueller, M.P. García-Cuellar, E. Maethner, and R.K. Slany. 2010. Leukemogenic transformation by HOXA cluster genes. *Blood*. 115:2910–2918. <https://doi.org/10.1182/blood-2009-04-216606>

Balasubramani, A., A. Larjo, J.A. Bassein, X. Chang, R.B. Hastie, S.M. Togher, H. Lähdesmäki, and A. Rao. 2015. Cancer-associated ASXL1 mutations may act as gain-of-function mutations of the ASXL1-BAP1 complex. *Nat. Commun.* 6:7307. <https://doi.org/10.1038/ncomms8307>

Berezniuk, I., H.T. Vu, P.J. Lyons, J.J. Sironi, H. Xiao, B. Burd, M. Setou, R.H. Angeletti, K. Ikegami, and L.D. Fricker. 2012. Cytosolic carboxypeptidase 1 is involved in processing α - and β -tubulin. *J. Biol. Chem.* 287: 6503–6517. <https://doi.org/10.1074/jbc.M111.309138>

Bononi, A., C. Giorgi, S. Patergnani, D. Larson, K. Verbruggen, M. Tanji, L. Pellegrini, V. Signorato, F. Olivetto, S. Pastorino, et al. 2017. BAP1 regulates IP3R3-mediated Ca^{2+} flux to mitochondria suppressing cell transformation. *Nature*. 546:549–553. <https://doi.org/10.1038/nature22798>

Bosch Grau, M., G. Gonzalez Curto, C. Rocha, M.M. Magiera, P. Marques Sousa, T. Giordano, N. Spassky, and C. Janke. 2013. Tubulin glycosylases and glutamylases have distinct functions in stabilization and motility of ependymal cilia. *J. Cell Biol.* 202:441–451. <https://doi.org/10.1083/jcb.201305041>

Carbone, M., H. Yang, H.I. Pass, T. Krausz, J.R. Testa, and G. Gaudino. 2013. BAP1 and cancer. *Nat. Rev. Cancer*. 13:153–159. <https://doi.org/10.1038/nrc3459>

Cimmino, L., I. Dolgalev, Y. Wang, A. Yoshimi, G.H. Martin, J. Wang, V. Ng, B. Xia, M.T. Witkowski, M. Mitchell-Flack, et al. 2017. Restoration of TET2 Function Blocks Aberrant Self-Renewal and Leukemia Progression. *Cell*. 170:1079–1095.e20. <https://doi.org/10.1016/j.cell.2017.07.032>

Dey, A., D. Seshasayee, R. Noubade, D.M. French, J. Liu, M.S. Chaurushiya, D.S. Kirkpatrick, V.C. Pham, J.R. Lill, C.E. Bakalarski, et al. 2012. Loss of the tumor suppressor BAP1 causes myeloid transformation. *Science*. 337: 1541–1546. <https://doi.org/10.1126/science.1221711>

Eddé, B., J. Rossier, J.P. Le Caer, E. Desbruyères, F. Gros, and P. Denoulet. 1990. Posttranslational glutamylation of alpha-tubulin. *Science*. 247: 83–85. <https://doi.org/10.1126/science.1967194>

Flach, J., S.T. Bakker, M. Mohrin, P.C. Conroy, E.M. Pietras, D. Reynaud, S. Alvarez, M.E. Diolaiti, F. Ugarte, E.C. Forsberg, et al. 2014. Replication stress is a potent driver of functional decline in ageing haematopoietic stem cells. *Nature*. 512:198–202. <https://doi.org/10.1038/nature13619>

Garnham, C.P., A. Vemu, E.M. Wilson-Kubalek, I. Yu, A. Szyk, G.C. Lander, R.A. Milligan, and A. Roll-Mecak. 2015. Multivalent Microtubule Recognition by Tubulin Tyrosine Ligase-like Family Glutamylases. *Cell*. 161: 1112–1123. <https://doi.org/10.1016/j.cell.2015.04.003>

Himburg, H.A., G.G. Muramoto, P. Daher, S.K. Meadows, J.L. Russell, P. Doan, J.T. Chi, A.B. Salter, W.E. Lento, T. Reya, et al. 2010. Pleiotrophin regulates the expansion and regeneration of hematopoietic stem cells. *Nat. Med.* 16:475–482. <https://doi.org/10.1038/nm.2119>

Hou, Y., W. Li, Y. Sheng, L. Li, Y. Huang, Z. Zhang, T. Zhu, D. Peace, J.G. Quigley, W. Wu, et al. 2015. The transcription factor Foxm1 is essential for the quiescence and maintenance of hematopoietic stem cells. *Nat. Immunol.* 16:810–818. <https://doi.org/10.1038/ni.3204>

Janke, C. 2014. The tubulin code: molecular components, readout mechanisms, and functions. *J. Cell Biol.* 206:461–472. <https://doi.org/10.1083/jcb.201406055>

Janke, C., and J.C. Bulinski. 2011. Post-translational regulation of the microtubule cytoskeleton: mechanisms and functions. *Nat. Rev. Mol. Cell Biol.* 12:773–786. <https://doi.org/10.1038/nrm3227>

Janke, C., K. Rogowski, D. Wloga, C. Regnard, A.V. Kajava, J.M. Strub, N. Temurak, J. van Dijk, D. Boucher, A. van Dorselaer, et al. 2005. Tubulin polyglutamylase enzymes are members of the TTL domain protein family. *Science*. 308:1758–1762. <https://doi.org/10.1126/science.1113010>

Liu, B., K.M. Yee, S. Tahk, R. Mackie, C. Hsu, and K. Shuai. 2014. PIAS1 SUMO ligase regulates the self-renewal and differentiation of hematopoietic stem cells. *EMBO J.* 33:101–113. <https://doi.org/10.1002/emboj.201283326>

Liu, B., B. Ye, X. Zhu, G. Huang, L. Yang, P. Zhu, Y. Du, J. Wu, S. Meng, Y. Tian, and Z. Fan. 2017a. IL-7R α glutamylation and activation of transcription factor Sall3 promote group 3 ILC development. *Nat. Commun.* 8:231. <https://doi.org/10.1038/s41467-017-00235-x>

Liu, B., B. Ye, L. Yang, X. Zhu, G. Huang, P. Zhu, Y. Du, J. Wu, X. Qin, R. Chen, et al. 2017b. Long noncoding RNA lncKdm2b is required for ILC3 maintenance by initiation of Zfp292 expression. *Nat. Immunol.* 18: 499–508. <https://doi.org/10.1038/ni.3712>

Makki, N., and M.R. Capecchi. 2010. Hoxal lineage tracing indicates a direct role for Hoxal in the development of the inner ear, the heart, and the third rhombomere. *Dev. Biol.* 341:499–509. <https://doi.org/10.1016/j.ydbio.2010.02.014>

Mashtalir, N., S. Daou, H. Barbour, N.N. Sen, J. Gagnon, I. Hammond-Martel, H.H. Dar, M. Therrien, and B. Affar. 2014. Autodeubiquitination protects the tumor suppressor BAP1 from cytoplasmic sequestration mediated by the atypical ubiquitin ligase UBE2O. *Mol. Cell*. 54:392–406. <https://doi.org/10.1016/j.molcel.2014.03.002>

Moran-Crusio, K., L. Reavie, A. Shih, O. Abdel-Wahab, D. Ndiaye-Lobry, C. Lobry, M.E. Figueroa, A. Vasanthakumar, J. Patel, X. Zhao, et al. 2011. Tet2 loss leads to increased hematopoietic stem cell self-renewal and myeloid transformation. *Cancer Cell*. 20:11–24. <https://doi.org/10.1016/j.ccr.2011.06.001>

Nakagawa, M.M., K. Thummar, J. Mandelbaum, L. Pasqualucci, and C.V. Rathinam. 2015. Lack of the ubiquitin-editing enzyme A20 results in

- loss of hematopoietic stem cell quiescence. *J. Exp. Med.* 212:203–216. <https://doi.org/10.1084/jem.20132544>
- Orkin, S.H., and L.I. Zon. 2008. Hematopoiesis: an evolving paradigm for stem cell biology. *Cell.* 132:631–644. <https://doi.org/10.1016/j.cell.2008.01.025>
- Pilarski, R., C.M. Cebulla, J.B. Massengill, K. Rai, T. Rich, L. Strong, B. McGillivray, M.J. Asrat, F.H. Davidorf, and M.H. Abdel-Rahman. 2014. Expanding the clinical phenotype of hereditary BAP1 cancer predisposition syndrome, reporting three new cases. *Genes Chromosomes Cancer.* 53:177–182. <https://doi.org/10.1002/gcc.22129>
- Platt, R.J., S. Chen, Y. Zhou, M.J. Yim, L. Swiech, H.R. Kempton, J.E. Dahlman, O. Parnas, T.M. Eisenhaure, M. Jovanovic, et al. 2014. CRISPR-Cas9 knockin mice for genome editing and cancer modeling. *Cell.* 159:440–455. <https://doi.org/10.1016/j.cell.2014.09.014>
- Rathinam, C., L.E. Matesic, and R.A. Flavell. 2011. The E3 ligase Itch is a negative regulator of the homeostasis and function of hematopoietic stem cells. *Nat. Immunol.* 12:399–407. <https://doi.org/10.1038/ni.2021>
- Rogowski, K., J. van Dijk, M.M. Magiera, C. Bosc, J.C. Deloulme, A. Bosson, L. Peris, N.D. Gold, B. Lacroix, M. Bosch Grau, et al. 2010. A family of protein-deglutamylating enzymes associated with neurodegeneration. *Cell.* 143:564–578. <https://doi.org/10.1016/j.cell.2010.10.014>
- Rossi, L., K.K. Lin, N.C. Boles, L. Yang, K.Y. King, M. Jeong, A. Mayle, and M.A. Goodell. 2012. Less is more: unveiling the functional core of hematopoietic stem cells through knockout mice. *Cell Stem Cell.* 11:302–317. <https://doi.org/10.1016/j.stem.2012.08.006>
- Sato, T., N. Onai, H. Yoshihara, F. Arai, T. Suda, and T. Ohteki. 2009. Interferon regulatory factor-2 protects quiescent hematopoietic stem cells from type I interferon-dependent exhaustion. *Nat. Med.* 15:696–700. <https://doi.org/10.1038/nm.1973>
- Takubo, K., N. Goda, W. Yamada, H. Iriuchishima, E. Ikeda, Y. Kubota, H. Shima, R.S. Johnson, A. Hirao, M. Suematsu, and T. Suda. 2010. Regulation of the HIF-1 α level is essential for hematopoietic stem cells. *Cell Stem Cell.* 7:391–402. <https://doi.org/10.1016/j.stem.2010.06.020>
- Tort, O., S. Tanco, C. Rocha, I. Bièche, C. Seixas, C. Bosc, A. Andrieux, M.J. Moutin, F.X. Avilés, J. Lorenzo, and C. Janke. 2014. The cytosolic carboxypeptidases CCP2 and CCP3 catalyze posttranslational removal of acidic amino acids. *Mol. Biol. Cell.* 25:3017–3027. <https://doi.org/10.1091/mbc.e14-06-1072>
- Tothova, Z., R. Kollipara, B.J. Huntly, B.H. Lee, D.H. Castrillon, D.E. Cullen, E.P. McDowell, S. Lazo-Kallanian, I.R. Williams, C. Sears, et al. 2007. FoxOs are critical mediators of hematopoietic stem cell resistance to physiologic oxidative stress. *Cell.* 128:325–339. <https://doi.org/10.1016/j.cell.2007.01.003>
- van Dijk, J., J. Miro, J.M. Strub, B. Lacroix, A. van Dorsselaer, B. Edde, and C. Janke. 2008. Polyglutamylolation is a post-translational modification with a broad range of substrates. *J. Biol. Chem.* 283:3915–3922. <https://doi.org/10.1074/jbc.M705813200>
- Wang, H., G. Liu, D. Shen, H. Ye, J. Huang, L. Jiao, and Y. Sun. 2015. HOXA1 enhances the cell proliferation, invasion and metastasis of prostate cancer cells. *Oncol. Rep.* 34:1203–1210. <https://doi.org/10.3892/or.2015.4085>
- Wilson, A., E. Laurenti, G. Oser, R.C. van der Wath, W. Blanco-Bose, M. Jaworski, S. Offner, C.F. Dunant, L. Eshkind, E. Bockamp, et al. 2008. Hematopoietic stem cells reversibly switch from dormancy to self-renewal during homeostasis and repair. *Cell.* 135:1118–1129. <https://doi.org/10.1016/j.cell.2008.10.048>
- Xia, P., S. Wang, Y. Du, G. Huang, T. Satoh, S. Akira, and Z. Fan. 2015. Insulin-InsR signaling drives multipotent progenitor differentiation toward lymphoid lineages. *J. Exp. Med.* 212:2305–2321. <https://doi.org/10.1084/jem.20150618>
- Xia, P., B. Ye, S. Wang, X. Zhu, Y. Du, Z. Xiong, Y. Tian, and Z. Fan. 2016. Glutamylolation of the DNA sensor cGAS regulates its binding and synthase activity in antiviral immunity. *Nat. Immunol.* 17:369–378. <https://doi.org/10.1038/ni.3356>
- Ye, B., C. Li, Z. Yang, Y. Wang, J. Hao, L. Wang, Y. Li, Y. Du, L. Hao, B. Liu, et al. 2014. Cytosolic carboxypeptidase CCP6 is required for megakaryopoiesis by modulating Mad2 polyglutamylolation. *J. Exp. Med.* 211:2439–2454. <https://doi.org/10.1084/jem.20141123>
- Ye, B., B. Liu, L. Hao, X. Zhu, L. Yang, S. Wang, P. Xia, Y. Du, S. Meng, G. Huang, et al. 2018. Klf4 glutamylolation is required for cell reprogramming and early embryonic development in mice. *Nat. Commun.* 9:1261. <https://doi.org/10.1038/s41467-018-03008-2>
- Yu, H., N. Mashtalir, S. Daou, I. Hammond-Martel, J. Ross, G. Sui, G.W. Hart, F.J. Rauscher III, E. Drobetsky, E. Milot, et al. 2010. The ubiquitin carboxyl hydrolase BAP1 forms a ternary complex with YY1 and HCF-1 and is a critical regulator of gene expression. *Mol. Cell. Biol.* 30:5071–5085. <https://doi.org/10.1128/MCB.00396-10>
- Zhu, H.H., K. Ji, N. Alderson, Z. He, S. Li, W. Liu, D.E. Zhang, L. Li, and G.S. Feng. 2011. Kit-Shp2-Kit signaling acts to maintain a functional hematopoietic stem and progenitor cell pool. *Blood.* 117:5350–5361. <https://doi.org/10.1182/blood-2011-01-333476>
- Zhu, X., Y. Xu, S. Yu, L. Lu, M. Ding, J. Cheng, G. Song, X. Gao, L. Yao, D. Fan, et al. 2014. An efficient genotyping method for genome-modified animals and human cells generated with CRISPR/Cas9 system. *Sci. Rep.* 4:6420. <https://doi.org/10.1038/srep06420>

Supplemental material

Xiong et al., <https://doi.org/10.1084/jem.20190974>

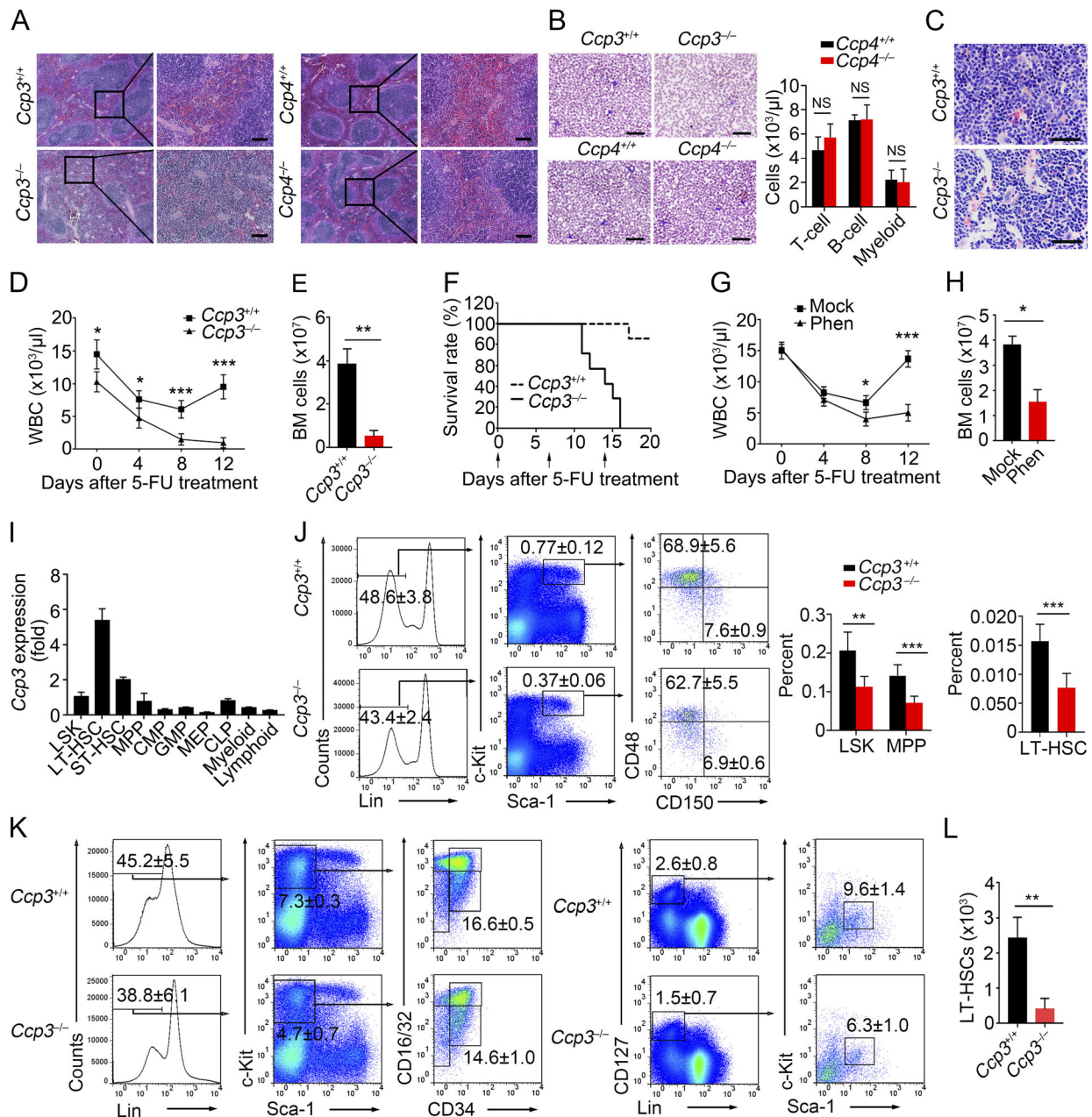


Figure S1. **Ccp3** deletion impairs HSC expansion. (A) H&E staining of spleen sections from *Ccp3*^{+/+} and *Ccp3*^{-/-} mice (left) and *Ccp4*^{+/+} and *Ccp4*^{-/-} mice (right). Scale bars, 50 μ m. (B) Left: Peripheral blood smears with Wright's staining of *Ccp3*^{+/+} and *Ccp3*^{-/-} (top) and *Ccp4*^{+/+} and *Ccp4*^{-/-} mice (bottom). Scale bars, 30 μ m. Right: T cells (CD3⁺), B cells (CD19⁺), and myeloid cells (CD11b⁺Gr-1⁺) of peripheral blood from *Ccp4*^{+/+} and *Ccp4*^{-/-} mice were analyzed with flow cytometry ($n = 6$). (C) H&E staining of BM sections from femurs of *Ccp3*^{+/+} and *Ccp3*^{-/-} mice. Scale bars, 50 μ m. (D and E) *Ccp3*^{+/+} and *Ccp3*^{-/-} mice were injected i.p. with 5-FU (150 mg/kg). Peripheral blood cells were counted every 4 d (D), and BM cells were counted 2 wk after 5-FU treatment (E). $n = 5$. (F) *Ccp3*^{+/+} and *Ccp3*^{-/-} mice were injected i.p. with 5-FU (150 mg/kg) every 7 d for three rounds, and survival rates were calculated ($n = 7$). (G and H) WT mice were injected i.p. with 5-FU (150 mg/kg) and then with phenanthroline (1.8 mg/kg) or PBS as a control every other day. Peripheral blood cells were counted every 4 d (G), and BM cells were counted 2 wk after 5-FU treatment (H). $n = 4$. (I) *Ccp3* mRNA expression levels in indicated lineages were detected by qPCR. Results were normalized to endogenous *Actb* gene ($n = 4$). (J) Flow cytometry gating strategies for LSKs (Lin⁻Sca-1⁺c-Kit⁺), MPPs (Lin⁻Sca-1⁺c-Kit⁺CD48⁺CD150⁻), and LT-HSCs (Lin⁻Sca-1⁺c-Kit⁺CD48⁺CD150⁺) from *Ccp3*^{+/+} and *Ccp3*^{-/-} mice. Total percentages of LSKs, MPPs, and LT-HSCs in a femur were counted ($n = 6$). (K) Flow cytometry gating strategies for HSPCs (Lin⁻Sca-1⁺c-Kit⁺), CMPs (Lin⁻Sca-1⁺c-Kit⁺CD34⁺CD16/32⁺), and CLPs (Lin⁻CD127⁺Sca-1^{low}c-Kit^{low}, right) from *Ccp3*^{+/+} and *Ccp3*^{-/-} mice. (L) *Ccp3*^{+/+} and *Ccp3*^{-/-} mice were injected i.p. with 5-FU (150 mg/kg). 1 wk later, LT-HSCs were analyzed by flow cytometry ($n = 4$). Results are shown as means \pm SD. *, $P < 0.05$; **, $P < 0.01$; ***, $P < 0.001$. Two-tailed Student's *t* test. Data in J and L are pooled from three independent experiments. Data in A-I, K, and L are representative of three independent experiments.

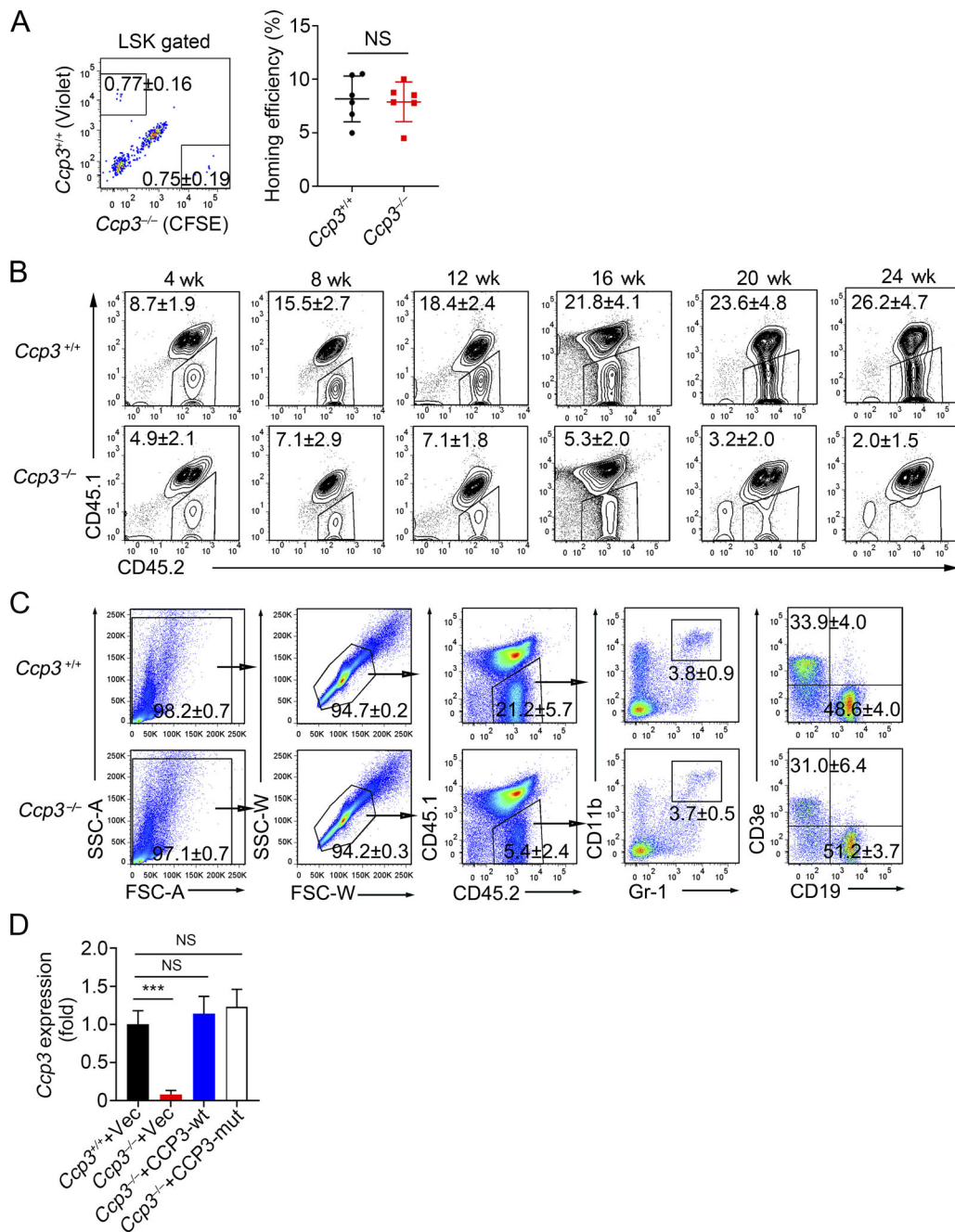


Figure S2. **CCP3 plays an intrinsic role in HSC self-renewal.** (A) LT-HSC homing assay. 2×10^3 LT-HSCs from $Ccp3^{+/+}$ and $Ccp3^{-/-}$ mice were sorted and stained with CellTrace violet and CellTrace CFSE, respectively, and then injected into lethally irradiated mice through tail vein injection. Homing of LT-HSCs in BM was analyzed by flow cytometry 18 h after transplantation, and homing efficiencies were calculated ($n = 6$). (B and C) 1×10^2 LT-HSCs from $Ccp3^{+/+}$ or $Ccp3^{-/-}$ mice were sorted and mixed with 5×10^5 BM helpers ($CD45.1^+CD45.2^+$) and then cotransplanted into lethally irradiated CD45.1 mice ($n = 5$). (B) Peripheral blood cells were analyzed by flow cytometry every 4 wk. (C) Peripheral myeloid cells ($CD11b^+Gr-1^+$), T cells ($CD3^+$), and B cells ($CD19^+$) derived from $Ccp3^{+/+}$ and $Ccp3^{-/-}$ LT-HSCs were further detected. (D) CCP3-wt or enzymatic inactive CCP3 (CCP3-mut) were overexpressed in $Ccp3^{-/-}$ LT-HSCs with pMYs retrovirus. GFP⁺ cells were sorted and CCP3-wt or CCP3-mut overexpression levels were analyzed by qPCR ($n = 4$). Results are shown as means \pm SD. ***, $P < 0.001$. Two-tailed Student's t test. Data are representative of three independent experiments.

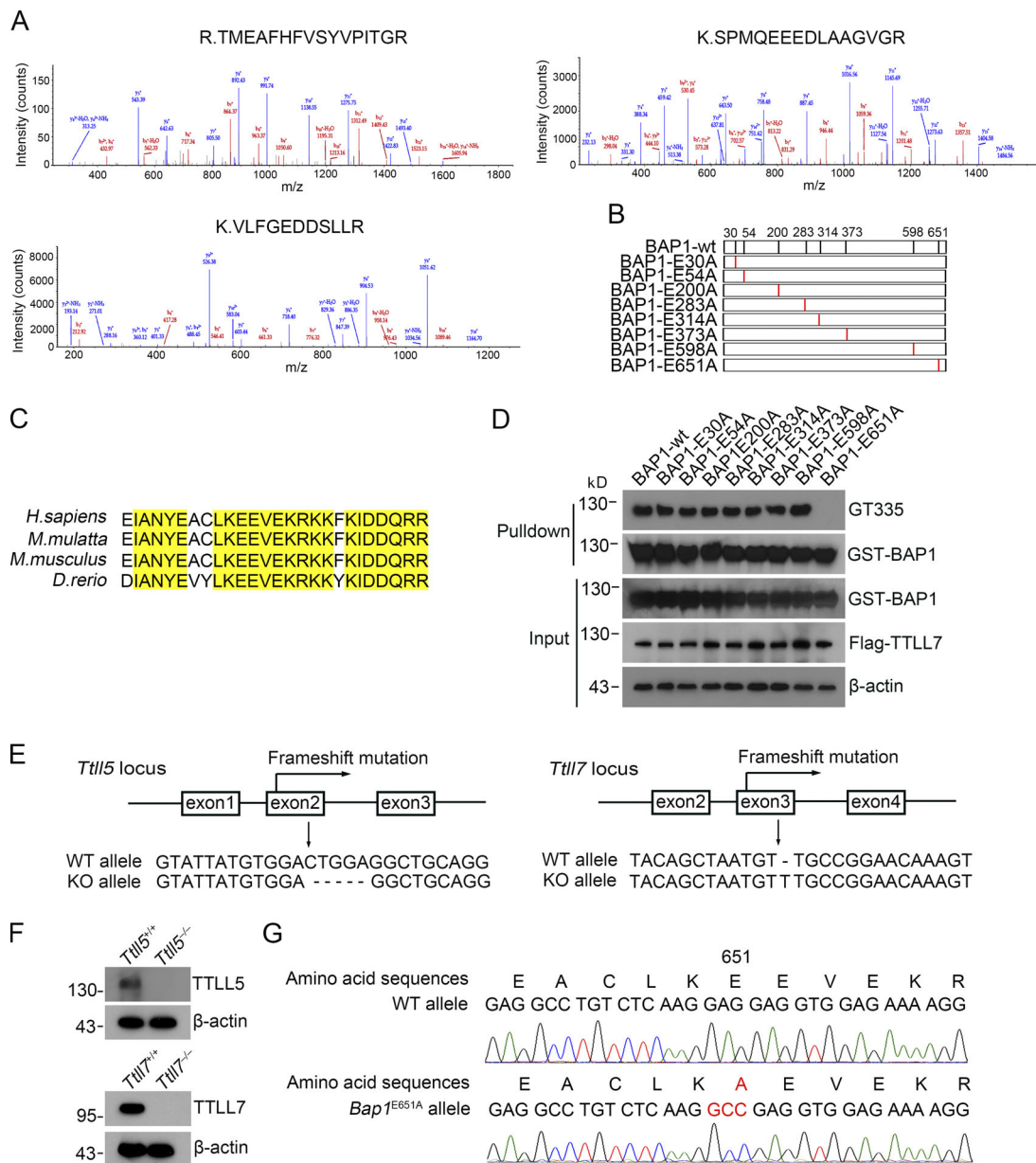


Figure S3. **BAP1 is glutamylated at E651 by TLL5 and TLL7.** (A) Recombinant CCP3-wt and enzymatic inactive CCP3 (CCP3-mut) were immobilized in Affi-Gel 10 resin and went through BM cell lysates. Eluted fractions were resolved by SDS-PAGE and stained by silver staining. A differential band around 95 kD in the CCP3-mut lane was cut for mass spectrometry. Tandem mass spectrometry profiles of representative BAP1 peptide sequences are shown. (B) Schematic representation of eight putative glutamate-rich sites in BAP1. (C) Amino acid alignment of BAP1 from different species. Conserved sequences are highlighted in yellow. (D) Flag-tagged TLL7 were transfected into HEK293T cells for 48 h. Cell lysates were incubated with recombinant WT BAP1 or various indicated mutants at 37°C for 2 h, followed by incubating with GST beads at 4°C for 1 h and Western blotting. Protein glutamylation was examined by immunoblotting with GT335 antibody. (E) Diagram of strategy for *Tll5* and *Tll7* knockout generation via CRISPR-Cas9 technology. 5-bp deletions of *Tll5* exon 2 and 1-bp insertion of *Tll7* exon 3, forming frameshift mutation, were identified by PCR and TA clone for DNA sequencing. (F) Western blot to confirm deficiency of TLL5 and TLL7. (G) *Bap1*^{E651A} knock-in mice were generated by CRISPR-Cas9 approach. Glutamine 651 of BAP1 was mutated to alanine (*Bap1*^{E651A}). Mutant mice were identified by PCR and TA clone for DNA sequencing. Data in A, D, F, and G are representative of three independent experiments.

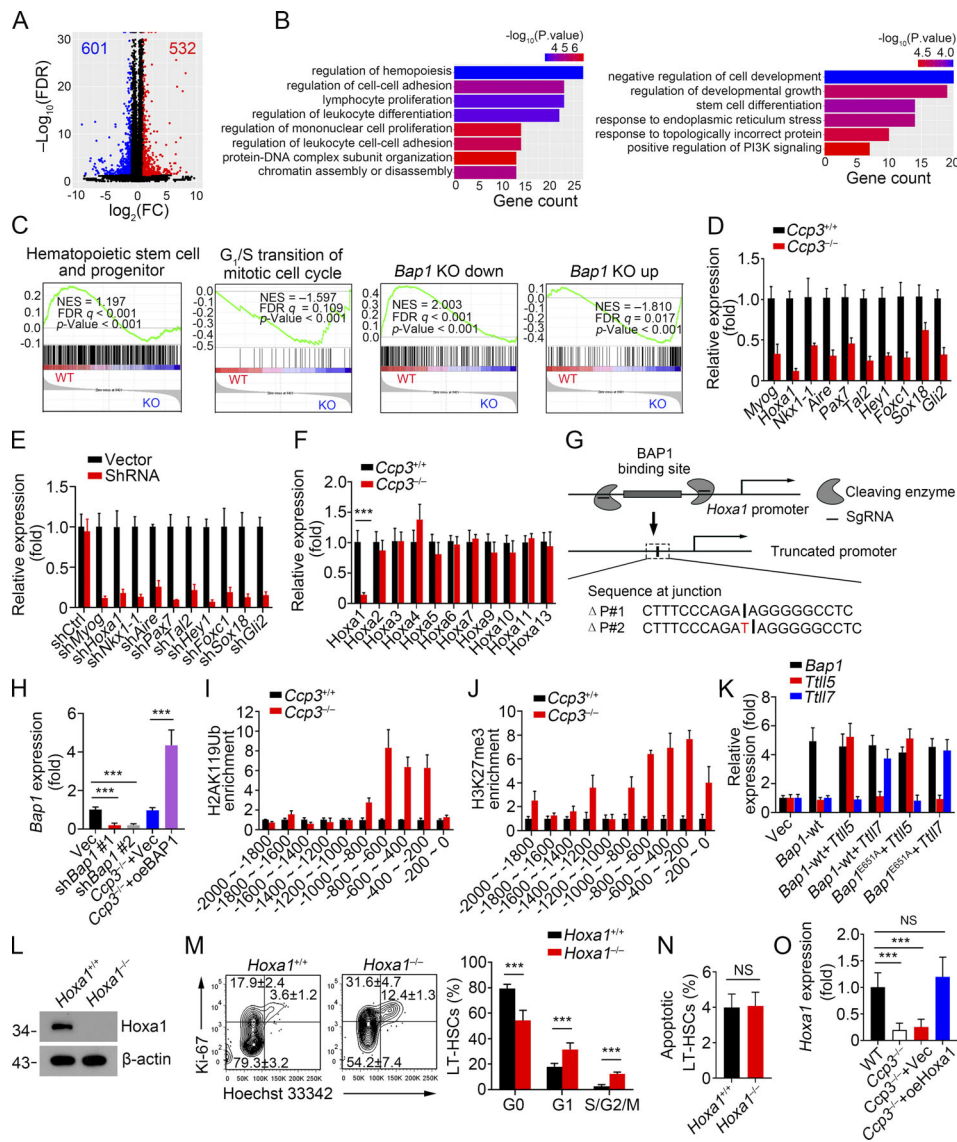


Figure S4. BAP1 targets on *Hoxa1* promoter to enhance *Hoxa1* expression. (A) Volcano plot of differentially expressed genes in *Ccp3*^{+/+} and *Ccp3*^{-/-} LT-HSCs. Genes whose expression changed more than twofold and whose false-discovery rate *q* value was <0.05 were selected as differentially expressed genes. (B) GO analysis of differentially expressed genes in *Ccp3*^{+/+} and *Ccp3*^{-/-} LT-HSCs. (C) GSEA of genes in *Ccp3*^{+/+} and *Ccp3*^{-/-} LT-HSCs enriched in selected gene sets, which were related to HSC and progenitor (first), G₁/S transition mitotic cell cycle (second), downregulated genes in BAP1-deficient LSKs (third), and upregulated genes in BAP1-deficient LSKs (fourth). Gene sets related to HSC and progenitor and G₁/S transition mitotic cell cycle were from the Molecular Signatures Database. Gene sets related to downregulated and upregulated genes in BAP1-deficient LSKs were based on transcriptomic data from GEO accession no. GSE40541. (D) RNA were extracted from *Ccp3*^{+/+} and *Ccp3*^{-/-} LT-HSCs (*n* = 4), and the top 10 downregulated genes were further analyzed by qPCR. Results were normalized to expression of endogenous *Actb* gene. (E) The top 10 downregulated genes in *Ccp3*^{-/-} LT-HSCs were knocked down by LMP microRNA-adapted retroviral system, followed by qPCR. Results were normalized to expression of empty vector infection (*n* = 4). (F) Genes in *HoxA* cluster in *Ccp3*^{+/+} and *Ccp3*^{-/-} LT-HSCs were analyzed by qPCR. Results were normalized to expression in *Ccp3*^{+/+} LT-HSCs (*n* = 4). (G) Schematic of deletion of BAP1 binding region of *Hoxa1* promoter with CRISPR-Cas9 technology. Indicated region deletions were identified by PCR and DNA sequencing. (H) LT-HSCs were infected with LMP retrovirus carrying shRNA against BAP1. BAP1 was overexpressed in *Ccp3*^{-/-} LT-HSCs with pMYs retrovirus, followed by qPCR. Results were normalized to expression of empty vector infection (*n* = 4). (I) Enrichment assessment of H2AK119Ub on indicated regions of *Hoxa1* promoter in *Ccp3*^{+/+} and *Ccp3*^{-/-} LT-HSCs. Enrichments were detected by qPCR with indicated primers and normalized to IgG enrichment value (*n* = 4). (J) Enrichment assessment of H3K27me3 on indicated regions of *Hoxa1* promoter in *Ccp3*^{+/+} and *Ccp3*^{-/-} LT-HSCs. Enrichments were detected by qPCR with indicated primers and normalized to IgG enrichment value (*n* = 4). (K) BAP1-wt or BAP1-mut with TLL5 or TLL7 was co-overexpressed in *Tll5*^{-/-}; *Tll7*^{-/-} LT-HSCs with pMYs retrovirus, followed by qPCR. Results were normalized to expression of empty vector infection (*n* = 4). (L) sgRNA targeting *Hoxa1* was designed according to an online tool and screened for efficiency. sgRNA targeting *LacZ* was used as a control. LT-HSCs sorted from Cas9 knock-in mice were infected with lentivirus including sgRNA and Cre recombinase expression, followed by cotransplantation with helper cells into lethally irradiated recipient mice. 1 mo later, GFP⁺ BM cells were sorted to analyze *Hoxa1* protein levels through Western blotting. (M) Cell cycle analysis of *Hoxa1*^{+/+} and *Hoxa1*^{-/-} LT-HSCs (*n* = 6). (N) Apoptosis analysis of *Hoxa1*^{+/+} and *Hoxa1*^{-/-} LT-HSCs (*n* = 6). (O) *Hoxa1* was overexpressed in *Ccp3*^{-/-} LT-HSCs, followed by qPCR. Results were normalized to expression of WT LT-HSCs (*n* = 4). Results are shown as means ± SD. *** *P* < 0.001 (two-tailed Student's *t* test). Data in M and N are pooled from three independent experiments. Data in D–F, H–L, and O are representative of three independent experiments. FDR, false-discovery rate; FC, fold change; NES, normalized enrichment score.

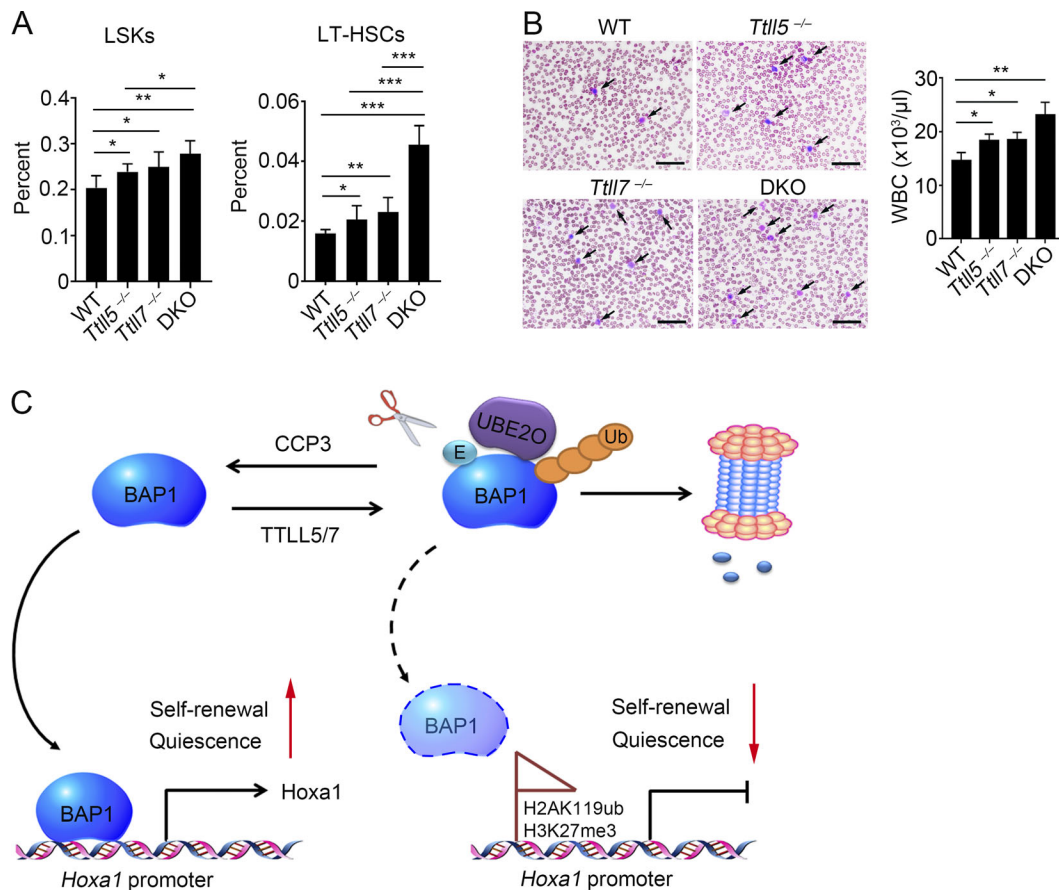


Figure S5. ***Ttl5* and *Ttl7* deficiencies promote HSC self-renewal.** (A) LSKs and LT-HSCs from WT, *Ttl5*^{-/-}, *Ttl7*^{-/-}, and *Ttl5*^{-/-};*Ttl7*^{-/-} (DKO) mice were detected by flow cytometry, and percentages per femur were calculated (*n* = 6). (B) Left: Peripheral blood smears with Wright's staining of WT, *Ttl5*^{-/-}, *Ttl7*^{-/-}, and DKO mice. The arrows indicate peripheral white blood cells. Right: Numbers of peripheral blood cells in indicated mice were calculated (*n* = 6). (C) Work model of BAP1 glutamylation in regulating HSC self-renewal. Results are shown as means ± SD. *, *P* < 0.05; **, *P* < 0.01; ***, *P* < 0.001. Two-tailed Student's *t* test. Data in A and B are pooled from three independent experiments.

Table S1. Hematopoietic cell counts in peripheral blood of *Ccp3*^{+/+} and *Ccp3*^{-/-} mice

Parameter	<i>Ccp3</i> ^{+/+} (<i>n</i> = 5)	<i>Ccp3</i> ^{-/-} (<i>n</i> = 5)	P value
WBC (x10 ⁶ /ml)	22.3 ± 4.5	10.0 ± 1.6	0.001
Lymph (x10 ⁶ /ml)	16.6 ± 3.9	6.5 ± 2.5	0.003
Mon (x10 ⁶ /ml)	0.7 ± 0.1	0.5 ± 0.1	0.005
Gran (x10 ⁶ /ml)	5.0 ± 0.7	2.9 ± 1.3	0.023
RBC (x10 ⁹ /ml)	10.2 ± 1.4	7.7 ± 1.1	0.018
HGB (mg/ml)	157.0 ± 13.6	128.2 ± 19.7	0.043

Hematopoietic parameters were analyzed using an XFA6030 automated hemocytometer (Slpoo). Cell numbers and percentages were counted for each population. Data are shown as means ± SD. Lymph, lymphoid cells; Mon, monocytes; Gran, granulocyte; HGB, hemoglobin.

Table S2. **sgRNA sequences used in this study**

Target gene	sgRNAs
<i>Ccp3</i>	5'-GGAGTATCAGCTAGGAAGAT-3'
<i>Ccp4</i>	5'-GCCTATACCTTCCCAGCCCC-3'
<i>Ttll5</i>	5'-GGGATCACCCATGTATTATG-3'
<i>Ttll7</i>	5'-GCCGGAACAAAGTTTGAAAT-3'
<i>Bap1^{E651A}-up</i>	5'-GCCCTAAGGTATACAATGT-3'
<i>Bap1^{E651A}-down</i>	5'-CAGCTGTCCTTGGGCAGTAG-3'
<i>Hoxa1</i>	5'-ATCCTTGGCAGTGGCGACTC-3'
<i>LacZ</i>	5'-TGCGAATACGCCACGCGAT-3'

sgRNAs were designed according to an online tool (<http://crispr.mit.edu/>) and purchased from Sangon. sgRNA targeting *LacZ* was used as a control.

Table S3. Sequences of primers used for genotyping and qPCR

Primers	Sequences
<i>Ccp3</i> KO (Forward)	5'-TCAGCTGATTCTATTGGTGACCC-3'
<i>Ccp3</i> KO (Reverse)	5'-TGACCTCACAGTGGTATGGC-3'
<i>Ccp4</i> KO (Forward)	5'-AGGCTGTGTGCATTCATTATC-3'
<i>Ccp4</i> KO (Reverse)	5'-AGAAGATCACAGTTGACCTGAAC-3'
<i>Ttl5</i> KO (Forward)	5'-GCCAAGTATGAGGTAGGGACA-3'
<i>Ttl5</i> KO (Reverse)	5'-GGTCATACCCAGATCCCCTT-3'
<i>Ttl7</i> KO (Forward)	5'-GTCACCGTTCGTAGCTTTAACC-3'
<i>Ttl7</i> KO (Reverse)	5'-CTCCAGAACCCTACTGCTTT-3'
<i>Bap1</i> ^{E651A} (Forward)	5'-CTTGAGTGGAGAGAAGTACTC-3'
<i>Bap1</i> ^{E651A} (Reverse)	5'-ATAGTTGTGGTCTTCGCTG-3'
<i>Hoxa1</i> KO (Forward)	5'-ATGGAGGAAGTGAGAAAGTTGGC-3'
<i>Hoxa1</i> KO (Reverse)	5'-TGGTGGTGGGCGAGCTGATCTG-3'
<i>Ccp1</i> qPCR (Forward)	5'-TGAAAGCTATCAGCCCTGG-3'
<i>Ccp1</i> qPCR (Reverse)	5'-GAGCTGGCGTCTGAAGGATG-3'
<i>Ccp2</i> qPCR (Forward)	5'-TCGAGAACCCGAGAAGTCTT-3'
<i>Ccp2</i> qPCR (Reverse)	5'-TGCTCCTCTCCACAATCTCT-3'
<i>Ccp3</i> qPCR (Forward)	5'-TGACTTGGATGAGGATTCCTTCA-3'
<i>Ccp3</i> qPCR (Reverse)	5'-GGGAAGAATGGGTACCAATAG-3'
<i>Ccp4</i> qPCR (Forward)	5'-CCAGCAGTGCCTATACCTTCC-3'
<i>Ccp4</i> qPCR (Reverse)	5'-TGCTCAGATCAGTTTCCAAGTC-3'
<i>Ccp5</i> qPCR (Forward)	5'-CTGCTCATTCTCGTCTCAGG-3'
<i>Ccp5</i> qPCR (Reverse)	5'-ATCGAGTCCTAATGCAAGGGA-3'
<i>Ccp6</i> qPCR (Forward)	5'-AGGCAGGCAATGATACAGGAA-3'
<i>Ccp6</i> qPCR (Reverse)	5'-GGTTACCACTTTCAAAGCAAGCA-3'
<i>Bap1</i> qPCR (Forward)	5'-CTCCTGGTGAAGATTTCCGGT-3'
<i>Bap1</i> qPCR (Reverse)	5'-GAGTGGCACAAGAGTTGGGAA-3'
<i>Hoxa1</i> qPCR (Forward)	5'-CCTGGAGTGTGTGGTCCAG-3'
<i>Hoxa1</i> qPCR (Reverse)	5'-AGCAACCACTGTAGTCCAGC-3'
<i>Myog</i> qPCR (Forward)	5'-GAGACATGAGTGCCTGACC-3'
<i>Myog</i> qPCR (Reverse)	5'-AGGCTTGGAAACCGGATAGC-3'
<i>Nkx1-1</i> qPCR (Forward)	5'-GACACTATGGACGGACGAGC-3'
<i>Nkx1-1</i> qPCR (Reverse)	5'-CGGCGTCTCCTACTGTTGAA-3'
<i>Aire</i> qPCR (Forward)	5'-AGACCATGGCAGCTTCTGTC-3'
<i>Aire</i> qPCR (Reverse)	5'-ATAGTGACCTGGGCTCCCTT-3'
<i>Pax7</i> qPCR (Forward)	5'-TCAAGCCAGGAGACAGCTTG-3'
<i>Pax7</i> qPCR (Reverse)	5'-TAGGCTTGTCCCCTTTCCAC-3'
<i>Tal2</i> qPCR (Forward)	5'-GTTCCAGCTCCTAGCAAGA-3'
<i>Tal2</i> qPCR (Reverse)	5'-CACCGCTCCCTGGTATTTGT-3'
<i>Hey1</i> qPCR (Forward)	5'-TAACCGGAGACTGAGCGTGA-3'
<i>Hey1</i> qPCR (Reverse)	5'-TCGTTGGGGACATGGAACAC-3'
<i>Foxc1</i> qPCR (Forward)	5'-AGTCGTGGTTAAGAGCGAGG-3'
<i>Foxc1</i> qPCR (Reverse)	5'-ATGATGGTCTCCACGCTGAA-3'
<i>Sox18</i> qPCR (Forward)	5'-GCTAGCAGCGCGTCTATTA-3'
<i>Sox18</i> qPCR (Reverse)	5'-TGGCATCTTTAGGCCACCAG-3'

Table S3. Sequences of primers used for genotyping and qPCR (Continued)

Primers	Sequences
<i>Gli2</i> qPCR (Forward)	5'-GGTGTGGACTCATTGCCTGA-3'
<i>Gli2</i> qPCR (Reverse)	5'-TGCACCAAATTTACTGCCTG-3'
<i>18S</i> (Forward)	5'-AACCCGTTGAACCCATT-3'
<i>18S</i> (Reverse)	5'-CCATCCAATCGGTAGTAGCG-3'
<i>Actb</i> (Forward)	5'-GGCTGTATCCCTCCATCG-3'
<i>Actb</i> (Reverse)	5'-CCAGTTGGTAACAATGCCATGT-3'
<i>Ttll1</i> qPCR (Forward)	5'-GAAGTGGGTCACTGACATTGAG-3'
<i>Ttll1</i> qPCR (Reverse)	5'-ACGTTGCGAATGGTTGAC-3'
<i>Ttll2</i> qPCR (Forward)	5'-GAGTTCACACCCCTGACATTC-3'
<i>Ttll2</i> qPCR (Reverse)	5'-GCATTTGTACCTACCCACGAGT-3'
<i>Ttll4</i> qPCR (Forward)	5'-TGGATGAGAACCTGAAACCT-3'
<i>Ttll4</i> qPCR (Reverse)	5'-TGGGGCTGCTGGAACCTAGA-3'
<i>Ttll5</i> qPCR (Forward)	5'-ACTCCCAGCTCCCATCTG-3'
<i>Ttll5</i> qPCR (Reverse)	5'-GGGGCATTGTGAGAACCG-3'
<i>Ttll6</i> qPCR (Forward)	5'-CTAACTGCCGGTATGACAGCG-3'
<i>Ttll6</i> qPCR (Reverse)	5'-AGTAGTCGGTCCAATAGAGAGTC-3'
<i>Ttll7</i> qPCR (Forward)	5'-CTCTGCCTCAAGATGGGGTTA-3'
<i>Ttll7</i> qPCR (Reverse)	5'-GTTCCGGCAACATTAGCTGTAA-3'
<i>Ttll9</i> qPCR (Forward)	5'-TGGAGTGTGAAAGGAAAAGAGA-3'
<i>Ttll9</i> qPCR (Reverse)	5'-TGCTCATCCATGTAGGTGTGG-3'
<i>Ttll11</i> qPCR (Forward)	5'-CCTGACCAACTACTCCCTGAA-3'
<i>Ttll11</i> qPCR (Reverse)	5'-GGGATGTCTGACTGGTAGAAAAC-3'
<i>Ttll13</i> qPCR (Forward)	5'-GGCCTGAAGGAAGTAGGGGA-3'
<i>Ttll13</i> qPCR (Reverse)	5'-CATGCCAGGGAAGTGTTGA-3'
<i>Hoxa2</i> qPCR (Forward)	5'-TACGAATTTGAGCGAGAGATTGG-3'
<i>Hoxa2</i> qPCR (Reverse)	5'-GTCGAGGTCTTGATTGATGAACT-3'
<i>Hoxa3</i> qPCR (Forward)	5'-TCAGCGATCTACGGTGGCTA-3'
<i>Hoxa3</i> qPCR (Reverse)	5'-GAGGCAAAGGTGGTTCACCC-3'
<i>Hoxa4</i> qPCR (Forward)	5'-GAAAGCACAACTCACAGCCC-3'
<i>Hoxa4</i> qPCR (Reverse)	5'-GTCTCGGGTTTACTTAGGGAAG-3'
<i>Hoxa5</i> qPCR (Forward)	5'-CTCATTTTGGGTCGCTATCC-3'
<i>Hoxa5</i> qPCR (Reverse)	5'-ATCCATGCCATTGTAGCCGTA-3'
<i>Hoxa6</i> qPCR (Forward)	5'-CACCCTCGGGCAATAACAAG-3'
<i>Hoxa6</i> qPCR (Reverse)	5'-GCCGTCAGGTTTGTACTGCT-3'
<i>Hoxa7</i> qPCR (Forward)	5'-TCCAGAATCGGCGCATGAAG-3'
<i>Hoxa7</i> qPCR (Reverse)	5'-ACGCTTTTCCAAGTGCCTG-3'
<i>Hoxa9</i> qPCR (Forward)	5'-GGCCTTATGGCATTAAACCTGA-3'
<i>Hoxa9</i> qPCR (Reverse)	5'-ACAAAGTGTGAGTGTCAAGCG-3'
<i>Hoxa10</i> qPCR (Forward)	5'-GGCAGTTCCAAAGGCGAAAAT-3'
<i>Hoxa10</i> qPCR (Reverse)	5'-GTCTGGTGCTTCGTGTAAGGG-3'
<i>Hoxa11</i> qPCR (Forward)	5'-TCTTCGCGCCAATGACATAC-3'
<i>Hoxa11</i> qPCR (Reverse)	5'-GGCTCAATGGCGTACTCTCT-3'
<i>Hoxa13</i> qPCR (Forward)	5'-TGGAAAGCTATCAGCCCTGG-3'

Table S3. Sequences of primers used for genotyping and qPCR (Continued)

Primers	Sequences
<i>Hoxa13</i> qPCR (Reverse)	5'-GAGCTGGCGTCTGAAGGATG-3'

Primers were designed with Primer 5 and purchased from Sangon.

Table S4. Sequences of primers used in ChIP assays

Loci	Sequences
-200 ~ 0 (Forward)	5'-TCCAAGTCAGCTCCGGG-3'
-200 ~ 0 (Reverse)	5'-GAATGTACAGTGCGCAAGAG-3'
-400 ~ -200 (Forward)	5'-AGAGATTTTCGGCCACAAGA-3'
-400 ~ -200 (Reverse)	5'-GCTGACTTGGAGCACTGGG-3'
-600 ~ -400 (Forward)	5'-TCTGCGCACGTCCCTCTA-3'
-600 ~ -400 (Reverse)	5'-GCCAAAATCTCTGCGTGG-3'
-800 ~ -600 (Forward)	5'-TTCCAGAGAGCTGGGTTCGTA-3'
-800 ~ -600 (Reverse)	5'-GGACGTGCGCAGAGGATTGA-3'
-1000 ~ -800 (Forward)	5'-AGCATGCTCCTGGGTCTCTA-3'
-1000 ~ -800 (Reverse)	5'-GAACCCAGCTCTCTGGGAAA-3'
-1200 ~ -1000 (Forward)	5'-TGTCCTCCACCTGCC-3'
-1200 ~ -1000 (Reverse)	5'-GGCCATCTGCCAACTTTAG-3'
-1400 ~ -1200 (Forward)	5'-CCAAGCTTAGAGTTGACGTGAC-3'
-1400 ~ -1200 (Reverse)	5'-GGTGTGAGACCGGCAG-3'
-1600 ~ -1400 (Forward)	5'-TTGCATTCTTCCCTTCCT-3'
-1600 ~ -1400 (Reverse)	5'-AGATGTCACGTCAACTCTAAGC-3'
-1800 ~ -1600 (Forward)	5'-CTACTCCCCGAAAGTGGGT-3'
-1800 ~ -1600 (Reverse)	5'-TCTATAGGAAGGGAAGAAGATGC-3'
-2000 ~ -1800 (Forward)	5'-GAGAGAGCCCTCACCCG-3'
-2000 ~ -1800 (Reverse)	5'-ACCCACTTTCGGGAGTAGTAT-3'

Primers were designed with Primer 5 and purchased from Sangon.

Table S5. Sequences for shRNAs used in this study

shRNA target gene	Sequences
<i>Myog</i> #1	5'-AGGAATTTAGCTGACTCCTTAA-3'
<i>Hoxa1</i> #1	5'-CGGCCCTGGCCACGTATAATAA-3'
<i>Hoxa1</i> #2	5'-AGCCACGTATAATAACTCCTTA-3'
<i>Nkx1-1</i> #1	5'-CCGTTCTACAGAAGAGAAAT-3'
<i>Nkx1-1</i> #2	5'-GCCATGTCCCAGAACAAGCAT-3'
<i>Aire</i> #1	5'-CCCTTCTCTTGAAACGGAAT-3'
<i>Aire</i> #2	5'-CCGACCTGGAGTCCCTCCTCAA-3'
<i>Pax7</i> #1	5'-CGTCCAGGTCTGGTTCAGTAA-3'
<i>Pax7</i> #2	5'-GGCTCTCAAGGTCTGGACAA-3'
<i>Tal1</i> #1	5'-CGGACAAACTGCTCTGTACATA-3'
<i>Tal1</i> #2	5'-CCCTGTGTATCTGTCATTGTAT-3'
<i>Hey1</i> #1	5'-ACCGACGAGACCGAATCAATAA-3'
<i>Hey1</i> #2	5'-CCGCCACTATGCTCAATGTTAA-3'
<i>Foxc1</i> #1	5'-CGCCTCTCACCTGTAAGATATT-3'
<i>Foxc1</i> #2	5'-CCCTATATGTCTGAATACTTTA-3'
<i>Sox18</i> #1	5'-ACGAATTTGACCAGTATCTCAA-3'
<i>Gli2</i> #1	5'-GGCACCAACCCTTCAGACTAT-3'
<i>Gli2</i> #2	5'-GGCCAGTATCCAGGATATAAT-3'
<i>Bap1</i> #1	5'-CCGCTGTGATTGATGATGATA-3'
<i>Bap1</i> #2	5'-CCCACGTCACCTTCCTGAGAAA-3'

Target sequences for RNA interference were designed according to MSCV-LTRmiR30-PIG system instructions.